NOVA SCHOOL OF SCIENCE & TECHNOLOGY

DEPARTAMENT OF MATERIALS SCIENCE

GONÇALO PEREIRA DA CUNHA VIDAL LOPES

Bachelor in Cell and Molecular Biology

NANOTRACERS – TRACKING THE (INTRA)CELLULAR FATE AND ORGANELLE TRAFFICKING OF GOLD NANOPARTICLES IN CANCER MODELS

MASTER IN BIOMATERIALS AND NANOMEDICINE

NOVA University Lisbon

June, 2024

NOVA SCHOOL OF SCIENCE & TECHNOLOGY

DEPARTAMENT OF MATERIALS SCIENCE

NANOTRACERS – TRACKING THE (INTRA)CELLULAR FATE AND ORGANELLE TRAFFICKING OF GOLD NANOPARTICLES IN CANCER MODELS

GONÇALO PEREIRA DA CUNHA VIDAL LOPES

Bachelor in Cell and Molecular Biology

Adviser: Pedro Miguel Ribeiro Viana Baptista
Full Professor, NOVA University Lisbon

Co-advisers: Maria Alexandra Núncio de Carvalho Ramos Fernandes
Associate Professor with Habilitation, NOVA University Lisbon

Examination Committee:

Chair: Luís Alexandre Almeida Fernandes Costa Branco,
Associate Professor, NOVA University Lisbon

Rapporteurs: João Carlos dos Santos Silva e Pereira de Lima,
Full Professor, NOVA University Lisbon

Adviser: Pedro Miguel Ribeiro Viana Baptista,
Full Professor, NOVA University Lisbon

MASTER IN BIOMATERIALS AND NANOMEDICINE

NOVA University Lisbon
June, 2024

NanoTracers - Tracking the (Intra)cellular fate and organelle trafficking of gold nanoparticles In cancer models

To my parents.

ACKNOWLEDGMENTS

The past year and a half were one of the most difficult times I experienced in my life. A series of events that repeatedly took me down, where I had never been, and to where I don't want to go back. This thesis marks the end of a cycle. It closes a door, putting these dark times in the past.
I would like to express my sincere gratitude to everyone that, directly or indirectly, lifted me up, and contributed to my personal growth, and to the completion of this work. Their assistance has been invaluable, and, without their support, this thesis would not come to fruition.
To Professor Pedro Viana Baptista, for the time, guidance, advises. In general, thanks for the opportunity and all the help throughout this entire journey.
To Professor Alexandra Fernandes for the kindness, all the support and advises along this journey.
To all members of lab 315, André, Beatriz, Daniela, Joana, Rúben, Sandra, Vasco, I am grateful for the companionship and all the enjoyable times shared in the lab, support and advises.
To FCT NOVA, for being my home for 6 incredible years. Here, I was challenged to always push my limits. I experienced unimaginable personal, scientific, and academic growth. Here, I found some of the people that are now on my closest circle.
To my friends, for always being there, and always supporting me.
To Clara, for the companionship, and all the patience, the strength and support, but most importantly for never giving up on me, and diving in the dark with me.
To my family, I thank all the opportunities, all the support and all the faith and love they give me everyday. Thank you for showing me that, even in the darkest of times, there is always a light to guide me.

Gonçalo Lopes

"Happiness can be found, even in the darkest of times, if one only remembers to turn on the light." - Albus Dumbledore

"I can do all things through Him who strengthens me." - Philippians 4:13

ABSTRACT

Cancer is a leading cause of mortality globally, claiming nearly 10 million lives in 2022. Therefore, developing novel, specific, and selective therapies is crucial. Nanotechnology is an interdisciplinary field and plays a key role by creating, manipulating, and studying materials at the nanoscale (1-100 nm) with unique properties. Nanomedicine, which applies nanotechnology to medicine, offers innovative theranostic solutions. Gold nanoparticles (AuNPs) are particularly promising for nanomedicine due to their distinctive physico-chemical and optical properties, making them ideal for imaging and drug delivery. Polyethylene glycol (PEG), an inert and non-toxic molecule with a thiol group in one end, has affinity to gold. Functionalizing AuNPs with PEG enhances their colloidal stability and allows further functionalization with other biomolecules. In this study, AuNPs were synthesized and functionalized with two bi-functional PEG molecules (PEG-COOH and PEG-NH_2) to enable further attachment of two fluorescent dyes: tetramethylrhodamine cadaverine (TAMRA) and fluorescein isothiocyanate (FITC). The stability of each nanoconjugate was tested at pH values from 5 to 8. AuNP@PEG-NH_2@FITC showed greater stability across pH variations than AuNP@PEG-COOH@TAMRA, which were highly unstable at lower pH levels. pH 7 was found to be the most suitable for dual functionalization with both dyes on a single AuNP.

Keywords: Gold Nanoparticles, Functionalization, TAMRA, FITC, Stability

Resumo

O cancro é uma das principais causas de morte a nível mundial, reclamando quase 10 milhões de vidas em 2022. Como tal, o desenvolvimento de novas formas de terapia, específicas e seletivas, é crucial. A nanotecnologia é uma área interdisciplinar e exerce um papel fulcral na criação, manipulação e estudo de materiais à nanoescala (1-100 nm), com propriedades únicas. A nanomedicina, que aplica a nanotecnologia à medicina, oferece novas soluções de teranóstico. As nanopartículas de ouro (AuNPs) são particularmente promissoras em nanomedicina, devido às suas distintas propriedades físico-químicas e óticas, fazendo delas ideais para imagiologia e entrega de fármacos. O polietileno glicol (PEG) é uma molécula inerte e não tóxica, com um grupo tiol numa das extremidades e com afinidade para o ouro. A funcionalização das AuNPs com PEG aumenta a sua estabilidade coloidal e permite a sua posterior funcionalização com outras biomoléculas. Neste trabalho, as AuNPs foram sintetizadas e funcionalizadas com duas moléculas bi-funcionais de PEG (PEG-COOH e PEG-NH_2), de forma a permitir a sua funcionalização com dois fluoróforos distintos: tetrametilrodamina cadaverina (TAMRA) e fluoresceína isotiocianato (FITC). A estabilidade de cada nanoconjugado foi testada em valores de pH entre 5 e 8. As AuNP@PEG-NH_2@FITC apresentaram maior estabilidade em variações de pH, do que as AuNP@PEG-COOH@TAMRA, que apresentaram elevada instabilidade para níveis de pH mais baixos. O pH 7 foi considerado o mais adequado para permitir a dupla funcionalização de uma única AuNP.

Palavras chave: Nanopartículas de Ouro, Funcionalização, TAMRA, FITC, Estabilidade

CONTENTS

LIST OF FIGURES

LIST OF TABLES

ABBREVIATIONS

Abs	Absorbance
AUC	Area Under the Curve
AuNPs	Gold Nanoparticles
AuNP@Citrate	Gold Nanoparticles with citrate capping
AuNP@PEG	PEGylated Gold Nanoparticles
AuNP@PEG-COOH@TAMRA	AuNPs functionalized with TAMRA
AuNP@PEG-NH_2@FITC	AuNPs functionalized with FITC
CCP	Clathrin-coated pits
CIE	Clathrin-Independent endocytosis
CME	Clathrin-Mediated Endocytosis
CT	Computed Tomography
Da	Dalton
DTNB	5,5'-dithio-bis(2-nitrobenzoic) acid
EDC	1-ethyl-3-(3-dimethylaminopropyl) carbodiimide hydrochloride
EPR	Enhanced Permeability and Retention
FDA	Food and Drug Administration
FITC	Fluorescein Isothiocyanate
FRET	Fluorescence Resonance Energy Transfer
MES	2-(N-morpholino)ethanesulfonic acid
MRI	Magnetic Resonance Imaging

MW	Molecular Weight
nm	Nanometer
NP	Nanoparticle
PAI	Photoacoustic Imaging
PEG	Polyethylene glycol
RT	Room Temperature
SDS	Sodium Dodecyl Sulfate
NSET	Nanosurface Energy Transfer
SPR	Surface Plasmon Resonance
Sulfo-NHS	N-hydroxysulfosuccinimide
TAMRA	Tetramethylrhodamine cadaverine
UV-Vis	Ultraviolet-Visible

1

INTRODUCTION

1.1 Cancer: A Global Nemesis

Ever since ancient times, Mankind has learned to live with diseases and to search for a way to cure them. Jumping ahead to the present day, we now understand that diagnosis and therapy are two key factors in the maintenance of health among the population. To achieve this, an early diagnosis is crucial, followed by a selective and specific therapeutic approach that ideally has minimal side effects. Cancer is the term used refer to diseases that are defined by an uncontrollable growth and spread of atypical cells. These cells are usually formed by genetic mutations, altering the normal cell cycle, and can be due to internal (genetic pre-disposition) or external factors (environmental exposures, viral infections or even lifestyle indicators). Cancer is a major cause of mortality, claiming nearly 10 million lives in 2022. Cancer accounts for almost one out of every six deaths globally, and this global health problem is far from being controlled, as its incidence is expected to sky rocket, rising by an astonishing 70% over the next 20 years[1–4]. In 2022, the number of new cancer cases was 19 976 499, and the number of 5-year prevalent cases was 53 504 187. These numbers show the high prevalence that cancer has in modern societies, justifying the great investment in fighting this disease. The research conducted over the last years, although opening several doors and making remarkable progress, is still far from comprehending the molecular processes of this illness. Therefore, the search for novel, selective and specific therapies is of utmost interest. Nanotechnology has the opportunity to play a role in this battle, offering a multitude of tools that can help cancer diagnosis and therapies[2,3].

1.2 Nanotechnology

Nanotechnology is an interdisciplinary domain that articulates several research areas, such as biology, chemistry, medicine and engineering[5]. The manipulation of nanomaterials has been happening long before this definition was established, mainly for decoration purposes[3,6,7], and its concept was primarily introduced, in an indirect way, in a talk by Richard Feynman, with the title

"There's plenty of room at the bottom" in a assembly of the American Physical Society at Caltech, in 1959.

Currently, nanotechnology can be described as the design, manipulation and study of convenient and functional materials (structures, devices and systems), at the nanoscale (1-100 nm)[8], and relies on the distinctive properties of such materials, namely optical, magnetic electronic and chemical[9]. These properties, allied to the fact that nanomaterials tend to possess high biological compatibility and stability, tuneable shape and size dispersion, as well as they are easily functionalised at the surface, allowed for the growth of this discipline, in the last decade, launching nanoparticles to be used in a wide range of applications[10]. Their high surface area to volume ratio is another property that differentiates nanomaterials from their bulk form. This, allied to their reduced size, similar to the functional elements and biological molecules present in living cells (ex. proteins and DNA/RNA) caused the interest to use nanoparticles in the biomedical field to increase, with applications in imaging and theranostics (the field that combines diagnostics to therapy)[6,9,11]. So far, the most common bioapplications for these materials are gene and drug delivery, labelling and detection, sensing and tumour targeting[12–14]. This broad spectrum of applications that could be used in the medical field, led to the emergence of a new "nano" field: nanomedicine.

1.3 Nanomedicine

As mentioned before, nanomedicine arose from the application of nanotechnology to the medical field[14], making use of the advantage provided by nanosized systems to improve theranostics[15]. Figure 1.1 depicts some examples of nanomaterials used on nanomedicine as: quantum dots[16], liposomes[17], noble metal nanoparticles[18], dendrimers and carbon nanotubes[19,20]. These nanomaterials have the ability to deliver molecules with low molecular weight in a more efficient and selective way, increasing clinical benefit while decreasing toxicity to healthy tissues[15,21,22]. Imaging applications are also of great interest for nanomaterials, allowing improved image detection and, therefore, improving diagnostics[22]. Additionally, there are efforts to develop theranostic agents, that will act on diagnostics and therapies at the same time.

Quantum dots, for example, are semiconductor nanoparticles exhibiting fluorescence, widely used for *in vivo* and *in vitro studies*, as they outperform greatly traditional organic dyes in most cases. In recent years, several studies resulted in improved stability, biocompatibility, specificity and other characteristics that make quantum dots a nanotechnology field that is experiencing rapid growth[23].

Liposomes were discovered in the 1960s and are a field of nanotechnology that has been undergoing significant investigation since. They are widely accepted as one of the most successful drug delivery systems known so far, being applied in several clinical trials[24].

Carbon nanotubes are intriguing nanodevices, with applications ranging from theranostics and imaging to drug delivery, due to their interesting mechanical properties. They consist of rolled up

graphene sheets, creating cylinders with diameters in the nanoscale, and have been extensively studied[20,25,26].

Metallic nanoparticles have been gaining interest due to their nontoxic and inert nature[27]. They are heavily used in biomedicine, due to their high potential in nanotechnology, as they possess an extensive variety of potential employments. For example, iron oxide NPs possess elevated magnetic properties, and have gained interest when applied to contrast agents for medical images (ex. MRI), or to magnetic separation processes, like DNA sequencing)[28]. Other possible applications of magnetic NPs are drug delivery or hyperthermia applications. Silver NPs are often used as antimicrobial agents, in wound dressings[28,29]. Gold nanoparticles, the object of this work, exhibit distinct optical, physical and chemical properties that make them not only suitable for biomedical use (ex. drug delivery, imaging, bionsensing), but also for environmental and industrial applications (acting as catalysts, for example)[28,29].

Figure 1.1 Different types of nanomaterials used in nanomedicine.

1.4 Gold Nanoparticles (AuNPs)

As mentioned earlier, nanomaterials have been used since medieval times. One of such examples is the application of colloidal AuNPs in cathedrals, owing to their optical properties, staining glass for the windows[30] (Figure 1.2). In 1857, Faraday was the first to comprehend such properties, describing that bulk and colloidal gold had different properties, attributing the red colour of gold nanoparticles to their colloidal nature[3,6,7]. Gold nanoparticles possess distinctive optical and physical-chemical properties [12,21,31,32], being one of the most widespread nanomaterial applied to nanomedicine, with theranostic purposes, such as drug delivery, *in vivo* imaging and cancer therapy[5,21,22].

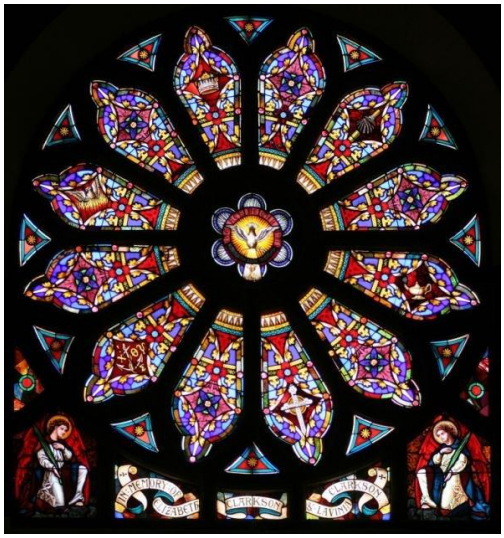

Figure 1.2 Stained glass containing gold nanoparticles[30]

1.4.1 Properties of AuNPs

As already mentioned, AuNPs' unique optical and electronic properties, easy surface functionalization, high biocompatibility and stability and controllable shape and size, have led to an increasing interest in their study, generating a broad variety of AuNPs based systems[10,12,21,33]. However, their reduced size is the most remarkable characteristic of AuNPs, increasing both their surface area to volume ratio and their stability in colloidal solutions[6]. Not only did Faraday attribute the red colour to colloidal AuNPs, but also related that characteristic colour to their size. From that moment, the interaction between AuNPs and light has been an interesting target of study[34].

When materials interact with light, several phenomena, like absorption, re-emission (ex. fluorescence) or scattering (ex. Raman scattering) can occur. These are all highly enhanced in the presence of AuNPs, due to the interaction between free electrons on the nanoparticles' surface and light. Since both AuNPs and light wavelengths are at the nanoscale, exposing AuNPs to light causes a collective oscillation of the conduction electrons on the surface of the nanoparticles. This is induced by their electromagnetic field, creating instantaneous dipoles. This phenomenon is called Surface Plasmon Resonance (SPR) and is one of the properties with utmost importance regarding AuNPs[6,35] (Figure 1.3).

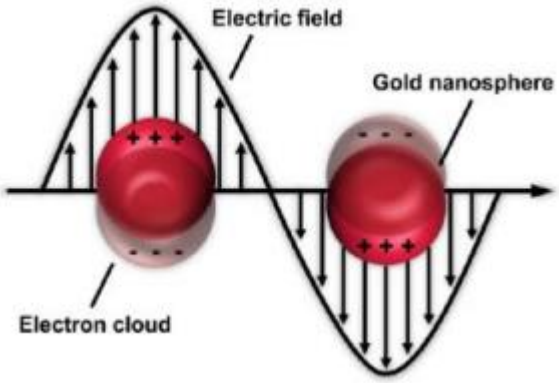

Figure 1.3 Schematic representation of the Surface Plasmon Resonance. After illumination at resonant wavelengths, AuNPs experience concomitant oscillation, due to the delocalization of the conduction band electrons on their surface[36].

The SPR effect results in high absorption coefficients and scattering properties, which allows for the use of spectroscopic techniques for optical detection methods and biological imaging by microscopic techniques[21,37]. The SPR frequency relies on the metallic species, shape and size of the nanoparticles and the medium's dielectric constant. This dependence is what makes the optical properties tuneable. For example, spherical AuNPs are completely symmetrical, resulting in a single SPR band. However, when analysing gold nanorods, this single band splits into two: a strong band in longer wavelengths, which results from the electrons' longitudinal oscillation, and a weaker band, in shorter wavelengths[38]. Focusing on the spherical AuNPs used in this work, the SPR absorption band is located around 520 nm. However, it redshifts with the increase in size, aggregation and formation of clusters, as the optical properties of AuNPs change[14,32]. Changes in pH, for example, change the dielectric constant of the medium, generating momentary dipoles, which reduces the repulsion between AuNPs, thus promoting their aggregation. As aggregation occurs, AuNPs maintain their typical behaviour, even though they are not chemically bonded, changing the colour of the solution to blue tones.. This is a direct consequence of the change occurring in the optical properties of the AuNPs, as their size increases, also increasing the wavelength of the SPR band. This aggregation-dependent change in colour has been significantly used in diagnostic tests[32,35,39,40].

1.4.2 Synthesis and Functionalization

AuNP synthesis often relies on the chemical reduction of Gold (III) to Gold (0), in the presence of a capping agent, that binds to the surface of the nanoparticle, blocking its growth and helping to stabilize in solution. By adjusting the conditions of the reaction (time, temperature, and capping agent), one can control the final AuNPs' morphology[32]. For example, AuNPs' shape and size results from the nature of the capping agent, temperature, salt concentration and the reactant addition

rates[41,42]. This is important because, given the fact that AuNPs are used for various purposes, there is the need to synthesize them with the appropriate size, shape, and surface functionalization[43]. In order to synthesize AuNPs with such variable characteristics, several synthesis methods have been reported over the years (ex. Seed Mediated Growth, Schmid and Brust-Schiffrin)[44]. These methods differ on capping and reduction agents, resulting in AuNPs with different sizes, shapes, in solutions that possess different stabilities and variable monodispersivity[45].

Faraday was the first to synthesize AuNPs, in 1857, reducing gold chloride (AuCl) with phosphorus. Nearly one century later, Turkevich et al. simplified Faraday's method, with the use of sodium citrate as a reduction agent[46]. Nowadays, the most widespread method for AuNP synthesis is based on the proposed by Turkevich in 1951[46], using citrate both as the reducing and capping agent. The diameter of the nanoparticles is determined by the careful control of the gold-citrate ratio.

Using this method, AuNPs with diameters ranging from 9 to 120 nm are obtained, with the diameter being inversely proportional to the citrate concentration. Besides that, citrate aids in stabilizing the AuNPs and allows further functionalization, as it is replaced by molecules with high affinity to gold with ease[32,33,43]. This is possible since citrate establishes weak interactions with the AuNPs (adsorption), being replaced by chemically bonded amine and thiol groups, that establish strong interactions with gold[47]. In nanomedicine, the ease to confer a biological function to inorganic nanostructures is of utmost importance[48].

Stability, functionality, and biocompatibility are all increased with the functionalization of AuNPs, as this process adjusts the properties of nanoparticle's surface by attaching different types of molecules. However, it is important to guarantee that these modifications do not alter the properties of the nanosystem[10,49]. For that, citrate-coated AuNPs need to be functionalized with a wide variety of biomolecules, such as PEG, antibodies, DNA/RNA oligonucleotides, peptides, drugs, fluorescent dyes and other molecules, depending on the purpose of the functionalized nanosystem[10,43,50]. Again, as there are plenty biomolecules that can be used with the goal of functionalizing AuNPs, with a multitude of final applications, there are also several methods to do so. However, one key aspect among all of them is that their primary goal is to improve both stability and affinity to the desired biomolecule.

The use of thiol groups to stabilize AuNPs was firstly described by Giersig and Mulvaney and stated that this stabilization was possible due to the strong interactions between a gold acid and a thiolated base. This allows the formation of gold-sulfur bonds and, therefore, thiol modified ligands are utilized for the stabilization of AuNPs[51].

Due to the presence of thiol groups in its chain, PEG is a often used macromolecule for *in vivo* and *in vitro* applications, as it has the advantage to be non-toxic and cleared for internal use in humans by the Food and Drug Administration (FDA)[52,53]. PEG also helps in stabilizing the AuNPs against biological fluids-induced aggregation, allowing the acquisition of long plasma half-lives, thus improving gene and drug delivery[10,49,54]. By using PEG, the adsorption of other biomolecules (ex.

Opsins) to the surface of the nanoparticles is also prevented, as the interaction between PEG chains and AuNPs creates a hydrophilic coating. This is helpful since the plasma molecules responsible for the recognition of strange bodies cannot bind to the AuNPs, allowing them to stay in circulation for longer periods of time[10,12,53–55] (Figure 1.4). PEG molecules may also act as a "bridge" for further functionalization, which is the case of this work. The other end of the PEG molecule may be a free carboxyl or amine group, that can be chemically bonded to other biomolecules, such as fluorescent dyes or tumoral markers, making PEG a spacer molecule[10,55,56].

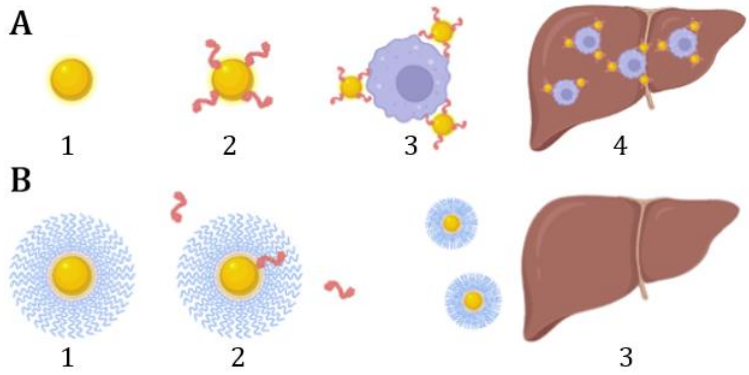

Figure 1.4 The Effect of opsonins in bare and PEGylated AuNPs. **A** – AuNPs (1) are coated with opsonins (2), leading to their association with macrophages (3) and, ultimately, liver sequestration (4). **B** – PEG-coated AuNP (1) prevent the adsorption of opsonins (2), inhibiting the macrophage association, allowing for long circulation periods and availability of AuNPs (3)[53].

This easy and versatile modification on the surface of AuNPs, making use of several different moieties, allied with AuNPs intrinsic unique optical properties, make them exceptional candidates for the development of novel theranostic methods for varied purposes[57].

This work involves the functionalization of AuNPs with fluorescent fluorophores. As so, it is important to understand the mechanisms behind the AuNPs' fluorescence quenching ability. Two possible theories to explain this interaction are: fluorescence resonance energy transfer (FRET) and nanosurface energy transfer (NSET). FRET states that both the energy donor and the receptor act as point dipoles. This means that, once exciting the donor (ex. AuNP), this will transfer energy to the receptor, non-radiatively. Dipole-dipole interactions conduct this transfer, in the transitions between the dipole moments of emission by the donor and absorption by the receptor, meaning that, spectroscopically, an overlap between the curves regarding emission and absorption is observed[58]. NSET is also based on non-radiative dipole-dipole interactions, yet contrarily to FRET, the acceptor is a nanosurface, composed of several point dipoles[58,59].

Comparing both theories, NSET possesses some advantages like a reduced signal to noise ratio and larger covering distances[60,61]. The spatial distance between donors and receptors is the main difference between FRET and NSET and is of critical importance in the design of FRET-based AuNP probes, as energy can only be transferred if both of them (donor and receptor) are close (1-20 nm). The energy transfer does not occur if donor and receptor are distant from each other[60].

Meanwhile, NSET can probe distances ranging from 1-40 nm[58]. FRET/NSET-based AuNP probes are utilized to quantify distances, or for the monitorization of various AuNP-biomolecule interactions, which can include structural or conformational analysis or quantification of a certain biomolecule's concentration in solution[58,60,62]. This broad spectrum of applications results from the combination of the distance range and length of biomolecules. Both FRET and NSET can be utilized for real-time *in situ* detection of different biomolecules, by toggling between "on" and "off" states through molecular association and dissociation or conformational changes[58].

1.4.3 AuNPs in Nanomedicine

AuNPs have been used in numerous fields of study, whether in *in vitro* assays, *in vivo/in vitro* imaging, and drug delivery. For example, if the main purpose of the study is to detect proteins or nucleotides, oligonucleotide-functionalized AuNPs can be used and detected by colorimetric detection methods, like UV-Visible Spectroscopy and Atomic Force Microscopy (AFM)[5]. However, if AuNPs are to be used for imaging purposes, they can be conjugated with contrast agents and be observed via light scattering imaging (ex. DLS), computed tomography (CT), magnetic resonance imaging (MRI) and surface-enhanced raman spectroscopy (SERS)[22,63].
Multifunctional AuNPs are a common target of study for their use in theranostic methods, as they combine imaging, diagnostics and therapy. These new systems are designed to overcome problems related to conventional drug delivery and therapeutic processes, which can include inefficiency in delivering the desired drug, and blocking native defence mechanisms. Additionally, theranostic nanosystems open doors that allow the assessment of drug delivery and release to be non-invasive, while assessing the therapeutic response and accumulation in the target site, at the same time[22,63,64].

1.5 AuNPs for Imaging

AuNPs relevance in biomedical imaging has been rising in recent years, due to the, already mentioned, distinct physicochemical and optical features[60,65]. AuNPs' versatility, high biocompatibility and stability and low indexes of toxicity turn them into good fit to be used for diverse imaging modalities, as contrast agents, theranostic agents or probes for molecular imaging[66]. This improves the detection and diagnosis of several conditions at cellular and molecular level[60,67]. The aforementioned SPR effect leads to strong absorption and scattering of light, dependent on the size, shape and aggregation state of AuNPs. For example, AuNPs with smaller diameters enhance imaging contrast in optical coherence tomography (OCT)[68], whereas larger or aggregated AuNPs are designed for the absorption of near-infrared (NIR) light for deep tissue imaging. Additionally, the easy and modulable surface functionalization of AuNPs allows the functionalization with several kinds of biomolecules (ex. peptides, DNA/RNA, antibodies, fluorescent dyes), allowing for

targeting of different tissues. Targeted AuNPs enhance their specificity and sensitivity, giving them highly valuable in the detection of different biomarkers and pathological conditions[60,69]. Functionalized AuNPs make use of different techniques, like surface-enhanced Raman scattering (SERS), where the AuNPs' surface significantly amplifies the Raman signal of nearby molecules, thus allowing the detection of low abundant biomarkers. Given all these factors, functionalized AuNPs can be used in different imaging modalities, such as optical imaging, computed tomography (CT), photoacoustic imaging (PAI) or magnetic resonance imaging (MRI).

1.5.1 Optical Imaging

The high scattering characteristics of AuNPs also make them of good used for optical imaging techniques, in three different aspects: direct observation of AuNPs inside the desired sample, tracking biomolecular activities and physiological functions and *in vivo* deep tissue imaging. The direct observation of AuNPs inside cells is possible via different microscopy techniques like dark field, differential interference and interferometric interference. Besides, optical imaging methods can be used to track the orientation and rotational motions of AuNPs, as these concepts are intimately related to biological functions. Techniques like surface-enhanced Raman spectroscopy and plasmon enhanced fluorescence are used to track ultra-sensitive biomolecules (ex. nucleic acids, proteins or metabolites). *In vivo* imaging is used for diagnostics, detecting tumours and other pathologies, through techniques such as two/multi-photon imaging, optical coherence tomography and photoacoustic imaging[68]. Optical imaging techniques provide high-resolution images of cellular components, while reducing photodamage to tissues, as AuNPs are excited by near-infrared light.

1.5.2 Computed Tomography (CT)

Regarding CT, AuNPs can be used as contrast agents, due to the high levels of X-ray absorption and flexible attenuation, high density and the broad spectrum of possible functionalization types[66]. This high attenuation will create a distinct signal on cancer tissues, non-typical for non-decorated, healthy cells. This will make the targeted tissue to be highly distinct and easy to observe[60,69,70]. As an X-ray/CT contrast agent, AuNPs can be categorized into three potential applications[71,72]: blood pool, active targeting and passive targeting. Blood pool contrast agents are created with the intent of staying in blood circulation for long periods of time, by limiting vascular endothelium diffusion[71,73]. Active targeting is based on delivering and maintaining the contrast agent in the specific targeted site, through functionalization with biomolecules with a specific affinity for that local[74,75]. Passive targeting, on the other hand, relies on the unspecific accumulation of AuNPs on cancer tissues due to the EPR effect, as AuNPs with appropriate size tend to accumulate with more ease in cancer tissues than in the surroundings[74,75]. Independently on the application, AuNP-based contrast agents need to be designed to the exact specifications of delivery, non-toxicity, targeting and contrast enhancement. This focused design will make AuNPs go to the

specific site, to cause no harm to the surrounding tissues, stay and accumulate where it is wanted and to increase X-ray attenuation, to show what it is supposed to be observed[71].

1.5.3 Photoacoustic Imaging (PAI)

PAI is an imaging modality used in biomedicine capable of giving functional information about tissue signatures at the cellular and molecular level, with resource to contrast agents. As so, due to their interesting and resourceful optical properties, AuNPs can be used as exogenous contrast agents[76]. Additionally, AuNPs have the ability to convert light into heat. This conversion generates ultrasonic waves that will be detected by photoacoustic imaging systems. PAI combines the high spatial resolution of optical imaging with the deep tissue penetration of ultrasounds, being the ideal imaging modality for imaging vascular structures, tumours and image-guided therapy[76].

1.5.4 Magnetic Resonance Imaging (MRI)

Although AuNPs are not inherently magnetic, they can enhance MRI contrast when combined with magnetic materials or through other innovative techniques. In regard to the combination with magnetic materials, AuNPs can be coated or attached with magnetic particles (ex. iron oxide nanoparticles). The new hybrid structure will benefit of the superparamagnetic properties of iron oxide and the high contrast provided by AuNPs accumulation in tissues[77]. Additionally, AuNPs allow functionalization with other biomolecules for active targeting. This functionalization localizes AuNPs in the area of interest, thus enhancing even more the contrast in MRI scans. AuNP-based systems can also be used for multimodal imaging agents, allowing for the combination with imaging modalities, like CT or optical imaging, which can improve diagnostic accuracy and enable comprehensive imaging studies[78].

1.6 AuNPs for Therapy

To this day, the most successful, and used, cancer therapies require invasive methods, whether it is assessed via chemotherapy, surgery, or radiation. In regard to chemotherapy, it poses great risk of toxicity to the adjacent healthy tissues, besides the possibility of resistance development by cancer cells. Radiation also has several side effects to the surrounding tissues, whether they are in the radiation beam's path or suffer from the bystander effect. Surgery, however, happens to be more controlled, although being the most invasive method. Besides, it cannot be performed in some clinical cases[44,79,80]. Therefore, the development of minimally invasive AuNP-based therapeutic approaches is of major importance.

Currently, there are four main types of AuNP-based therapeutic approaches to cancer[81]:

- **Photothermal Therapy:** Uses near-infrared light and relies on the conversion of photons to thermal energy, increasing the intracellular temperature, thus inducing cell death. AuNPs will absorb the emitted energy, converting it to heat. It has applications in cancer

treatments and combination therapies. Some advantages of photothermal therapy are the targeted treatment, real-time monitoring and the fact that it is minimally invasive[44,82];

- **Photodynamic Therapy:** Involves the combination of light and photosensitizers (light-sensitive drugs, sensitive to specific wavelengths of light, becoming activated when targetted), aiming to selectively destroy targeted cells. It is used in cancer treatments, as well as, in non-cancerous conditions (ex. age-related degeneration of the macula). It is also minimally invasive and allows for a targeted and repeatable treatment[83];
- **Radiotherapy:** Consists on the enhancement of cancer cells' radiosensitivity. AuNPs amplify the radiation's effects, producing more reactive electrons when exposed to radiation, causing an increase in DNA damage. It has the advantage of increasing efficacy, enhancing the effects of radiation, and minimizing the harm on healthy tissues[84];
- **Drug Delivery:** AuNPs are used as vectors for the delivery of molecules (ex. TNF-α, Tamoxifen and Doxorubicin) into a target[5,63], enhancing the precision and efficacy of treatments. Drug delivery AuNPs can be used in cancer therapies (delivering chemotherapeutic agents to tumours), gene therapy (delivering genetic material to specific cells, for editing or silencing) or in anti-inflammatory treatments (targeting inflamed locations in diseases like arthritis)[85].

One of the biggest setbacks concerning drug delivery nanosystems is exactly the targeting to the exact desired site. Normally, AuNPs used in nanomedicine, achieve the region of interest by one of two means: active or passive targeting. Regarding cancer tissues, AuNPs tend to target the tumour the passive way, taking advantage of the Enhanced Permeability and Retention (EPR) effect. The EPR effect happens because of the known abnormal characteristics of tumorous tissues. Their fast growth rate is dependent on the equally fast development of a blood supply, causing the blood vessels to be poorly vascularized and to have large fenestrations. This results in the discharge of AuNPs to the interstitial space and, therefore, AuNPs accumulate more in cancer tissues than in healthy ones. Moreover, solid tumours are known to have low lymphatic drainage, which helps even more the accumulation of AuNPs. Normally, to improve this tendency, AuNPs are also functionalized with specific targeting agents (ex. antibodies, oligonucleotides, proteins), varying according to the desired target/biomarker[22,33,63]. This shows that AuNPs possess a tremendous potential to be used in cancer treatments, as many efforts have been conducted to enhance traditional methods and develop more selective ones, thus protecting healthy tissues[80,81].

With that said, it is clear that AuNPs are a strong tool for applications in the biomedical field. Nonetheless, they still possess some limitations. Although being considered biocompatible, AuNPs' toxicity depends on factors like size and shape of the nanosystem, as well as the functionalization of the surface. Due to this, the biocompatibility and toxicity of the nanosystems must always be assessed prior to their utilization. Additionally, in order to translate these AuNP-based systems into clinical procedures, it is necessary to fully comprehend the mechanisms by which AuNPs interact with biological tissues[63,86].

1.7 Cell Internalization of AuNPs

In order to study the intracellular fate of the AuNPs, firstly the possible internalization processes must be understood. In this area, nanomedicine has been developing multifunctional nanoparticles, as vectors for theranostics, imaging agents and drug delivery, in a way that they would improve traditional therapeutics that suffered from inappropriate delivery[63]. In regard to drug delivery, AuNPs need to interact with a specific tissue, cell population or intracellular component. Therefore, AuNPs' biocompatibility and pharmacokinetics must be understood, in order to better understand their behaviour and improve drug delivery, keeping in mind that each nanoconjugate will have its own properties, varying its biocompatibility levels[15,63]. For this reason, understanding the internalization mechanisms of AuNPs has become extremely important over the years[63,86]. These kind of studies are of utmost importance to assess toxicity, understand, increase and manipulate accumulation on the targets and to improve the design on AuNPs, making them more efficient[9,87]. Additionally, it is important to learn how to target intracellular components, rather than only tissues or cell types, depending on the final destination of the nanoparticles and their function.

That said, and for the progress of nanomedicine, it is essential to conduct quantitative and qualitative studies on the internalization mechanisms of AuNPs, as they are dependent on their physicochemical properties, as well as the nature of the target[15,86].

1.7.1 Physicochemical properties of AuNPs Affecting Internalization

1.7.1.1 Size

AuNPs' size plays a key role in their internalization. Research suggests that, AuNPs with 50 nm diameter show higher internalization rates than larger and smaller ones[9], as result of a competition between diffusion kinetics and the process of membrane wrapping that happens in endocytosis. Studies show that AuNPs smaller than 50 nm need to cluster together, thus yielding enough free energy for membrane wrapping to happen[87,88]. Larger nanoparticles require a slower wrapping rate, because of the slower diffusion of plasma membrane receptors[87,88]. With that in mind, the AuNPs' size can be tuned, uniformized and stabilized, in order to correctly assess the role size plays on internalization mechanisms[15,89].

1.7.1.2 Shape

Shape is another characteristic that influences AuNPs' internalization: longer gold nanorods are less internalized than shorter ones, although their surface charge is identical. Additionally, in comparison to spherical AuNPs, these are more easily internalized, being taken up 500% more. These shape-induced differences in cell uptake can be explained due to the fact that the elongated nature of the nanorods requires longer times of membrane wrapping during the internalization process[88,90,91].

1.7.1.3 Surface Charge

Surface charge is intimately related to the biomolecules attached to AuNP's surface. As the plasma membrane is negatively charged, AuNPs with positive surfaces will stick to it, possessing higher internalization rates, than negatively charged and neutral surface charges. Additionally, targeting specific membrane molecules (ex. proteins or lipids) can also improve cellular uptake[89,92].

1.7.2 Internalization Mechanisms

All mammalian cells communicate with the surrounding environment through endocytosis, being this a critical process. Through endocytosis, cells internalize a multitude of chemical and biological compounds (ex. molecules, ions, proteins and nutrients), being also involved in motility and inter-cellular communication[86,93]. Traditionally, the endocytic pathways are divided into two main classes: phagocytosis and pinocytosis. Independently of the pathway, endocytosis is based on four fundamental concepts[93]:

- Specific binding to the membrane surface;
- Membrane pinching off and forming vesicles;
- Vesicle closing and detachment from the membrane;
- Intracellular trafficking of the formed vesicle.

1.7.2.1 Phagocytosis

This unspecific endocytic pathway only occurs on specialized phagocytic cells (ex. macrophages and dendritic cells), and is responsible for the uptake of large particles (larger than 5 μm), such as cell debris, pathogens and dead cells[86]. As it was afore mentioned, this process starts with the specific recognition at the membrane surface, inducing the formation of a phagosome. This phagosome will then mature and fuse with lysosomes, ultimately leading to degradation[15,93].

1.7.2.2 Pinocytosis

Pinocytosis refers to the uptake of fluids and solutes, and is still a debatable topic, under ongoing research, regarding its division. This division is based on the role clathrin plays on the process. As such pinocytosis is divided into clathrin-mediated endocytosis (CME) and clathrin-independent endocytosis (CIE)[15]. Clathrin is a protein present in the cytosol, responsible for the formation of coated pits, associated with adaptor proteins, that are responsible for the coordination of clathrin nucleation, near the site where the particles are being internalized.

1.7.2.2.1 Clathrin-Mediated Endocytosis (CME)

Being the principal internalization mechanism responsible for nutrient uptake, is the most studied pathway. It allows the internalization of nanoparticles in the 150-200 nm range[15,88], and is again initiated with their binding to the membrane, forming clathrin coated pits (CCP). After that, the pits form vesicles, that are now pinched off the membrane by dynamin, forming clathrin coated vesicles (CCV). Then, clathrin will depolymerize, and the particles are clustered into endosomes.

Endosomes will then fuse with lysosomes, thus inducing degradation. In some cases, particles are released in the cytosol and avoid degradation[15,93].

1.7.2.2.2 Clathrin-Independent Endocytosis (CIE)

Clathrin-independent endocytosis is, as the name implies, an endocytic pathway that doesn't require the participation of clathrin. This last category is divided in:

- **Caveolae-mediated endocytosis –** responsible for a multitude of biological functions, thus being the most studied mechanism. Caveolae are plasma membrane microdomains rich in cholesterol, and are characterized by the presence of the proteins caveolin-1 and caveolin-2. In this process, caveolin is present on the invagination of the plasma membrane in the form of a striated-coat. Then, caveosomes are formed and nanoparticles can be released in the cytosol or be degraded in the lysosomes. However, lysosomal degradation is usually bypassed, making this the most adequate mechanism of intracellular delivery[15,93,94].
- **Macropinocytosis –** this process in independent of clathrin and caveolae, being triggered by the activation of tyrosine kinase receptors, by growth factors, and being responsible for the uptake of larger particles (up to 5 μm). In micropinocytosis, a large amount of external fluid is internalized, through the formation of a waving sheet-like extension of the membrane, forming large vesicles, known as macropinosomes[15,88].

1.7.3 Assessment of Internalization Mechanisms

There are several ways one can assess the internalization mechanism of AuNPs. These different methods can be used solely or combined and rely on colocalization of endocytic biomarkers[95], knockdown of specific proteins[96] or specific exclusion of internalization pathways by endocytic inhibitors, that specifically exclude the endocytic pathways[15,96–98]. Colocalization of intracellular AuNPs relies on the differential labelling of organelles or intracellular compartments. This allows the analysis of colour distribution, within the cell, by fluorescent microscopy. This technique can be used in live cell imaging, which constitutes an advantage. However, it can be unprecise as the fluorescent markers can show continuous areas of fluorescence, that could overlap and camouflage the signal from other markers[97]. The use of endocytic markers presents several advantages that make it a better fit for the assessment of internalization mechanisms, such as the short exposure periods required and the fact that it is a more affordable approach[99]. Nonetheless, regular endocytic markers are not often selective, regarding specific pathways[15]. Endocytic pathways can also be assessed with resource to pharmacological inhibitors. This approach assumes that the inhibitors will have particular effects on a given endocytic pathway, but that's not always the case. For example, dynasore inhibits the dynamin function, in several different endocytic pathways[97,98].

In order to understand the intracellular fate of AuNPs, firstly it is necessary to comprehend the biological process behind it. After internalization of AuNPs, these are mainly found in endocytic vesicles, that will fuse forming early endosomes, that will mature into late endosomes, and

ultimately into lysosomes[100]. Along maturing stages, an acidification of the pH inside these vesicles is observed, which could induce aggregation or disrupt the colloidal stability of AuNPs. Current microscopy techniques, like fluorescence and transmission electron microscopy (TEM) techniques, while widely used, cannot capture real-time live cell images, and the sample preparation is a complex process, that can damage samples and degrade imaging quality of subcellular structures. Specifically, TEM is a microscopy technique that operates transmitting a beam of electrons through an ultra-thin sample, creating highly detailed images, allowing for the observation of fine cellular structures and nanoparticles within cells[101,102]. Due to their high electron density, AuNPs are of good use in TEM as it provides a strong contrast against cellular background, making them appear as dark spots in the resulting images, as can be seen in Figure 1.5[103].

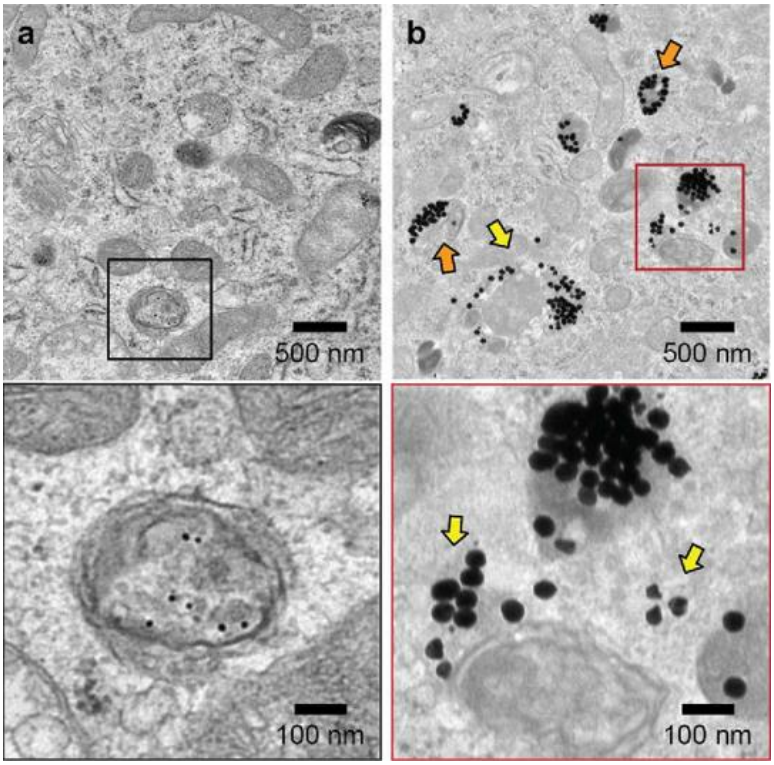

Figure 1.5 TEM images of AuNPs within cells. AuNPs exert high contrast, appearing as dark spots, independently on their size (**a** – 13 nm; **b** – 50 nm)[103].

As mentioned, sample preparation is complex and involves several steps like cell culture, fixation (preserves cellular structures), embedding in resin (provides support for ultra-thin sectioning), and staining (contrast enhancement)[101]. Although providing high resolution, high contrast and detailed images, TEM possesses several challenges, like a very complex sample preparation, the possibility for the unwanted introduction of artifacts during sample preparation, that could affect the interpretation of images, and damage of the biological samples due to prolonged exposure to the electron beam[102]. Furthermore, confocal microscopy is limited by the diffraction limit, which prevents the acquisition of precise nanoscale imaging of organelles[104,105]. A real-time tracking of the intracellular fate of AuNPs involves the assessment of intracellular movement, by tracking the dynamic behaviour of molecules, organelles, or other cellular compounds (like AuNPs) within

living cells. These processes often use fluorescent probes in different techniques, where the fluorescence is measured directly or indirectly. Fluorescence Correlation Spectroscopy (FCS) is a potent, sensitive analytical method, used to study the dynamics of fluorescent molecules, in real-time[106]. By measuring the fluorescence intensity variations, within a small and defined observation volume, FCS can provide information on diffusion properties, chemical reaction kinetics and molecular concentrations and interactions. This technique is especially useful in nanomedicine, as it allows the investigation of biomolecules in living cells, with high temporal resolution. Live cell imaging, on the other hand, is a dynamic method that allows the observation and recording the behaviour of biomolecules within a cell, in real-time[107]. Resourcing to fluorescence microscopy and fluorescent probes, live cell imaging allows the tracking of cellular processes, like organelle dynamics, within a living cell. This technique provides critical insights into the functioning of cells, and their interaction with biomolecules, enabling the study of physiological conditions with high spatial and temporal resolution. As there is an acidification of the intra-vesicle environment, during the endocytic pathways, pH-dependent fluorescent probes can be used in order to track the intracellular fate of AuNPs. For example, lysosomes can be tracked with resource to LysoTracker dyes, fluorescent dyes, specifically designed for the visualization of this organelle in live cells. Its acidophilic nature makes them accumulate in acidic environments, increasing the fluorescent intensity in lower pH values[108]. LysoTracker dyes are highly specific, versatile and easy to use in live cell imaging, making them an essential tool in cell biology, for the study of lysosomal dynamics. Another example of a fluorescent dye with similar characteristic is the pHrodo dye, also increasing their fluorescence intensity as the pH decreases, and are used as general pH indicators, with in organelles or cytosol[109].

1.8 Objectives

In this work, AuNPs will be functionalized with 2 different fluorescent fluorophores (TAMRA and FITC), in order to assess the possibility of designing an AuNP-based probe, functionalized with both dyes, capable of tracking the intracellular fate of AuNPs, allowing their detection within cells by fluorescence microscopy, in real-time, and visualizing transportation vesicles and organelles. This way, it is possible to track their movement and localization over time[106,107,110,111]. This process allows for a real-time understanding of the cellular response to AuNPs.

The TAMRA molecule is not pH-sensitive, as its properties do not change with variations of pH[112,113]. However, FITC is pH sensitive[114–116], being used as an indicator, when conjugated with nanoparticles, in pH-dependent drug delivery studies. The fluorescent intensity of FITC decreases in lower pH values, due to protonation of its fluorescein moiety, quenching its fluorescent capacity.

As mentioned, AuNPs are of a still increasing importance on the nanomedicine field. Therefore, understanding the interaction between them and cells is of crucial significance, in order to

optimize their design. The main objective of this project was to develop a probe that could be used to track AuNPs and trace their intracellular fate in cancer models, using two different fluorophores (TAMRA and FITC). For that, several tasks were defined:

- Synthesis of AuNPs;
- Functionalization and characterization of AuNPs with PEG;
- Functionalization and characterization of AuNPs with fluorophores, independently;
- Functionalization and characterization of AuNPs with both fluorescent dyes on the same nanoparticle;
- Assess the fate of the functionalized AuNPs within cells and tissues;
- Clarify the pathway AuNPs take from outskirts of a 3D tumour to the core and inside cells.

Functionalization with FITC required the design of a new protocol, whereas the functionalization with TAMRA followed an established protocol, with some fine tunings.
Due to personal issues and constraints, the objectives had to be re-adapted[1].

[1] Due to sick leave, a time suspension was granted.

2

MATERIALS AND METHODS

2.1 Equipment, Material and Reagents

Table 2.1 Equipment used for the realization of the experimental work.

Equipment	Company
UV-Vis Spectrophotometer UV Mini-1240	Shimadzu, Germany
Cary Eclipse Fluorescence Spectrophotometer	Agilent, USA
Sigma 3-16K Centrifuge	Sartorius, Germany
Sigma 1-14 Mini-Centrifuge	Sartorius, Germany
Shaker	GFL, Germany
Eclipse Ti Microscope	Nikon, Japan
Intensilight C-HGFI Epi-Fluorescence Illuminator	Nikon, Japan

2.1.1 Material

- Current laboratory material
- Quartz absorption cell – 105.202-QS (Hellma, Germany)
- Quartz precision cell – 105.251-QS (Hellma, Germany)
- Polystirol/Polystirene cuvette (SARSTEDT, Germany)

2.1.2 Reagents

- **Carbonate buffer 0.1 M pH 9** – Prepared by adding 91 mM of Sodium bicarbonate (Honeywell Fluka, USA), [$CHNaO_3$; MW 84.01 Da] and 9.002 mM of Sodium carbonate anhydrous (Sigma-Aldrich, USA), [Na_2CO_3; MW 105.99 Da];

- **5,5′-Dithiobis(2-nitrobenzoic acid) [DTNB]** (Sigma-Aldrich, USA), [$C_{14}H_8N_2O_8S_2$, MW 396.35 Da);
- **Fluorescein isothiocyanate (FITC)** (Sigma-Aldrich, USA), [$C_{21}H_{11}NO_5S$; MW 389.39 Da].
- **Gold chloroauric acid 99.999%** (Sigma-Aldrich, USA), [$HAuCl_4$, MW 339.785 Da];
- **MES buffer 2.5 mM pH 5.9** (Sigma-Aldrich, USA), [$C_6H_{13}NO_4S$; MW 195.24 Da];
- **Phosphate buffer 0.5 M pH 7/8.5** - Prepared by adding 288.55 mM of Sodium phosphate dibasic (Sigma-Aldrich, USA), [Na_2HPO_4, MW 141.96 Da] and 211.45 mM of Monosodium phosphate (Sigma-Aldrich, USA), [NaH_2PO_4, MW 119.98 Da];
- **Phosphate buffer saline** – Prepared by adding 1.37 M of Sodium chloride (Sigma-Aldrich, USA), [NaCl; MW 58.44 Da], 27 mM of Potassium chloride (Sigma-Aldrich, USA), [KCl; MW 74.55 Da], 100 mM of Sodium Phosphate dibasic (Sigma-Aldrich, USA), [Na_2HPO_4, MW 141.96 Da] and 18 mM of Potassium phosphate monobasic (Sigma-Aldrich, USA), [KH_2PO_4, MW 136.09];
- **Polyethylene glycol (PEG)** (Iris Biotech, Germany), [HS-PEG(8)-COOH, MW 458.57 Da];
- **Polyethylene glycol (PEG)** (Sigma-Aldrich, USA), [HS-PEG(2K)-NH_2, MW 2000 Da];
- **Sodium citrate tribasic dihydrate, ≥ 99%** (Sigma-Aldrich, USA), [$HOC(COONa)(CH_2CO\text{-}ONa)_2.2H_2O$; MW 294.10 Da];
- **Sodium Dodecyl Sulfate (SDS)** (Sigma-Aldrich, USA), [$NaC_{12}H_{25}SO_4$, MW 288.38 Da];
- **Tetramethylrhodamine cadaverine (TAMRA)** (Life-Technologies, USA), [$C_{30}H_{34}N_4O_4$; MW 514.623 Da];

2.2 Synthesis of Gold Nanoparticles

AuNPs were synthesized by the citrate reduction method[57,117], with the gold chloroauric acid being the gold supply and the sodium citrate acting as the reducing agent. All the glass material needed to conduct the synthesis process was immersed in *aqua regia* overnight, and then washed with milli-Q H2O. Milli-Q H2O was also used to prepare all solutions.

In a 250 mL round bottom flask, 150 mL of 2.2 mM Sodium Citrate were brought to boil, with vigorous stirring. When in reflux, 1 mL of 25 mM $HAuCl_4$ were added. The solution was kept in reflux, for approximately 10-20 minutes, until it turned reddish, from a characteristic yellow. After that, the solution was left to cool down, with continuous stirring, and then stored at RT, protected from light.

Synthesized AuNPs were analysed via UV-Visible Spectroscopy.

2.3 Functionalization of Gold Nanoparticles

2.3.1 AuNP@PEG-COOH@TAMRA

AuNPs were functionalized with a bi-functional PEG molecule, that had a thiol group at one end and a carboxyl group at the other end (PEG-COOH). As a consequence, amine groups present in

the TAMRA molecule, would react and bond to the carboxyl groups and, therefore, conjugating the AuNPs with the dye.

2.3.1.1 Functionalization with PEG

The purpose was to cover 30% of the AuNPs' surface. For that, given that 0.01 $mgmL^{-1}$ of PEG_COOH is necessary to obtain 100% saturation of the surface, a concentration of 0.003 $mgmL^{-1}$ was used. So, 10 mL of an aqueous solution containing 10 nM AuNPs, 0.003 $mgmL^{-1}$ PEG-COOH, and 0.028% (v/v) SDS, was prepared. The solution was then left for incubation, with continuous stirring, for 16 hours, on a GLF shaker 3006.

To remove possible unbound PEG-COOH molecules, the solution was centrifuged for 2 times, at 14000 g, 4ºC, for 45 minutes, and the supernatants were removed, reserved and replaced by Milli-Q H2O. Then, the supernatants were also centrifuged in the same conditions, and the unbound PEG-COOH chains were quantified by Ellman's Assay.

2.3.1.2 Functionalization with TAMRA

AuNP@PEG-COOH were then functionalized with TAMRA, a red fluorescent dye, by EDC and sulfo-NHS coupling reaction. To do so, a master mix containing 21 nM AuNP@PEG-COOH, 1.25 $mgmL^{-1}$ sulfo-NHS, and 0.312 $mgmL^{-1}$ EDC in MES buffer (2.5 mM, pH 5.9) was prepared, and incubated for 30 minutes, at room temperature, with continuous stirring. Then it was centrifuged for 30 minutes, at 14000 g, 4ºC. The supernatant was removed and replaced by MES. Then, in a 1:1 PEG-COOH:TAMRA ration, TAMRA was added to mixture that was incubated at room temperature for 16 hours, with continuous stirring. After that, samples were centrifuged 2 times, for 45 minutes, at 14000 g, 4ºC. supernatants were removed, reserved, and replaced by MES buffer.

AuNP@PEG-COOH@TAMRA were analysed via UV-Vis Spectroscopy, Fluorescent Spectroscopy and Fluorescence Microscopy. Supernatants were analysed by Fluorescent Spectroscopy, in the same conditions as the AuNPs, mentioned in Section 2.6.1.

2.3.2 AuNP@PEG-NH_2@FITC

Isothiocyanates are electrophile groups, reactive towards a variety of nucleophiles, as amines. They react well with amines under alkaline conditions, and are stable in aqueous conditions, as well as in most solvents. As such, a PEG molecule, containing a thiol group in one end and an amine in the other, was used to functionalize AuNPs and link FITC, a fluorescent green dye. The functionalization method was optimized in the lab, as throughout the whole process, AuNPs presented high instability[118–120].

2.3.2.1 Functionalization with PEG

Given that information, $1*10^{-11}$ mol of AuNP were taken of the stock solution and centrifuged for 15 minutes, 14000 g. the supernatant was removed. A PEG sample was prepared ate the same

time by dissolving 0.0025 g PEG in 20 uL DMSO, and diluted in 990 uL of water. Then, 5 uL of a stock solution of 6% SDS (v/v) was added to the mixture. AuNPs were resuspended in the PEG sample and incubated for 10 minutes with continuous stirring. After 10 minutes, 12.5 uL of a stock solution of 2 M NaOH was added, and the solution was left for incubation for 16 hours, with continuous stirring.

2.3.2.2 Functionalization with FITC

The functionalized AuNP@PEG-NH_2 Samples were then centrifuged for 30 minutes, at 14000g, 4ºC, and resuspended in Carbonate Buffer (0.1 M, pH 9). 0.0005 g FITC were dissolved in 20 uL DMSO. From the original FIT-C solution, 2 uL were taken and diluted 100 times in Carbonate Buffer, immediately before use. From the diluted sample, 10 uL were added to the AuNP@PEG-NH2. Then, 12.5 uL of NaOH 2M were added, and the samples were left to incubate in the dark, with continuous stirring, for 4 hours. After incubation, samples were centrifuged once, for 30 minutes, at 14000 g, 4ºC. Supernatants were removed, reserved and replaced by Phosphate Buffer (pH 8.5, non salt).
AuNP@PEG-NH2@FITC were analysed via UV-Vis Spectroscopy, Fluorescent Spectroscopy and Fluorescence Microscopy. Supernatants were analysed by Fluorescent Spectroscopy, in the same conditions as the AuNPs, mentioned in Section 2.6.2.

2.4 UV-Visible Spectroscopy

Synthesized and functionalized AuNPs were characterized with resource to UV-Vis Spectroscopy (400-800 nm), using absorption cells and polystirol/polystyrene cuvettes, both with 1 cm optical path.

2.5 Ellman's Assay

The Ellman's assay relies on the reaction between free thiol groups with DTNB, resulting in a yellow solution*. DTNB reacts with a thiol, forming a thiol-TNB adduct, and the concomitant release of 5-thio-2-nitrobenzoic acid (TNB). Then, the quantification of free thiol groups is based on the release of TNB, measures spectrophotometrically at 412 nm. For that, samples with known concentrations of PEG were prepared, in the presence of DTNB. After 10 minutes samples were analysed by UV-Vis spectroscopy, from 300 to 600 nm[121,122].

2.6 Fluorescence Spectroscopy

Fluorescence emission was assessed via fluorescence spectroscopy, using precision cells. All tests were conducted at RT, although each fluorophore required distinct conditions.

2.6.1 AuNP@PEG-COOH@TAMRA

For the TAMRA functionalized AuNPs the excitation wavelength was 543 nm, the recording frequency range 550-700 nm, at 30 nm/min with a photomultiplier potency of 800 V.

2.6.2 AuNP@PEG-NH_2@FITC

For the FITC functionalized AuNPs the excitation wavelength was 488 nm, the recording frequency range 490-600 nm, at 30 nm/min with a photomultiplier potency of 800 V.

2.7 Fluorescence Microscopy

10 nM of each AuNP species were prepared, and then 100 μL were placed on plain microscope slides. Then, samples were analysed via fluorescence microscopy, with an attached camera. Images were collected with resource to the NIS-Elements software, by Nikon. The exposure times were 10-50 ms for the bright field images and 10-20 s for the fluorescence ones. All readings were taken in the dark, at RT, varying only the light source (visible or UV).

2.8 pH Stability Assessment

To study the effect of pH on the nanoconjugates, samples with 10 nM AuNP and variable pH values were prepared. The desired pH values were obtained by diluting a previously prepared PBS 10x PBS solution, into PBS 1x with pH values of 5, 6, 7, and 8. After that, AuNPs were resuspended in each pH sample, and absorbance and fluorescence spectra were obtained after 2, 4, 6, 16, and 24 hours.

3

Results and Discussion

AuNPs are considered a central piece to a multitude of applications in nanomedicine[32,123,124]. Particularly, AuNP-based systems are being more and more used in theranostics[125]. As mentioned earlier, gold nanoparticles (AuNPs) present unique features that increment their *in vivo* circulation, necessary for these kind of applications[8]. As such, the interest of AuNP-based systems has sky rocketed in the last years, therefore increasing the need to study their internalization mechanisms and interaction with living systems. Given that, the objective of this work was to functionalize AuNPs with two different fluorophores, thus allowing for the characterization of cell uptake and tracing the intracellular fate of such nanosystem, under different conditions.

3.1 Synthesis of Gold Nanoparticles

Normally, AuNPs are synthesized by reducing Au3+ to Au0. For that to happen, there needs to be a reducing, capping/stabilizing agent, that will prevent aggregation and increase stability, as well as a "quality control" to the growth and size of AuNPs[7,41]. For example, when the capping agent is present in lower concentrations, there are fewer ions available, resulting in reduced stabilization of the nanoparticles. This, in turn, causes the smaller particles in the reaction system to coalesce[7,41]. As for the synthesis process, this project used the method proposed by Turkevich et al. in 1951, that allows the formation of AUNPs with significant monodispersity and with diameters ranging from 10-20 nm. It uses chloroauric acid ($HAuCl_4$) and sodium citrate both as a reducing and capping agent[7,41,117].

The AuNP synthesis was successful, and the resulting AuNPs were characterized by UV-Visible spectroscopy. UV-Visible spectroscopy is a technique that permits the assessment of the AuNPs' optical properties, resulting from the presence of the SPR band, that relies on size, shape, interparticle distance and the surrounding medium[126]. The SPR effect is observable in the form of a characteristic absorption band at around 519 nm[37]. Figure 3.1 shows the absorption spectrum obtained for the synthesized AuNPs, with a maximum peak at 519 nm, as expected. Additionally, the SPR peak is symmetrical, narrow, and well-defined. These are all possible indicators of the

monodispersivity of colloidal spherical AuNPs[127–129], as they all have the same size and shape*. In a polydisperse system, the variation on particle sizes leads to a variation in SPR wavelengths, thus broadening the SPR band. With the analysis of the absorption spectrum, the concentration of the AuNPs was also calculated, using the Lambert-Beer Law, assuming an absorption coefficient of 2.33×10^8 $M^{-1}.cm^{-1}$ for the SPR peak[130]*. AuNPs were also characterized by microscopy, confirming the high monodispersivity and spherical shape of AuNPs.

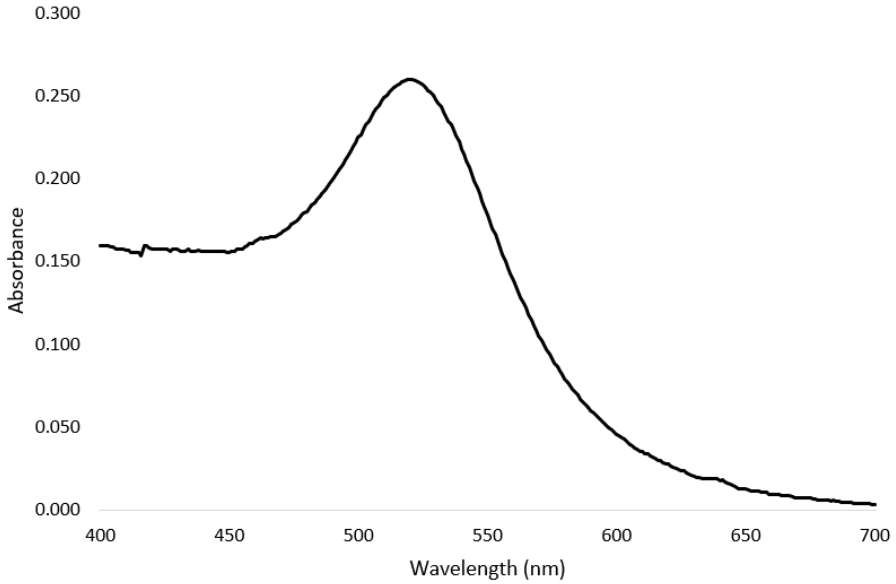

Figure 3.1 UV-Visible spectrum of the synthesised AuNPs, for wavelengths ranging from 400-700 nm, with the SPR peak centered at 519 nm

3.2 Functionalization of Gold Nanoparticles

After the AuNPs were synthesised, they were functionalized. One of the objectives of this work was to functionalize AuNPs with two different fluorophores: TAMRA and FITC. For that, AuNPs were primarily functionalized with PEG-COOH and PEG-NH_2, respectively. Figure 3.2 depicts a schematic representation of the functionalization process.

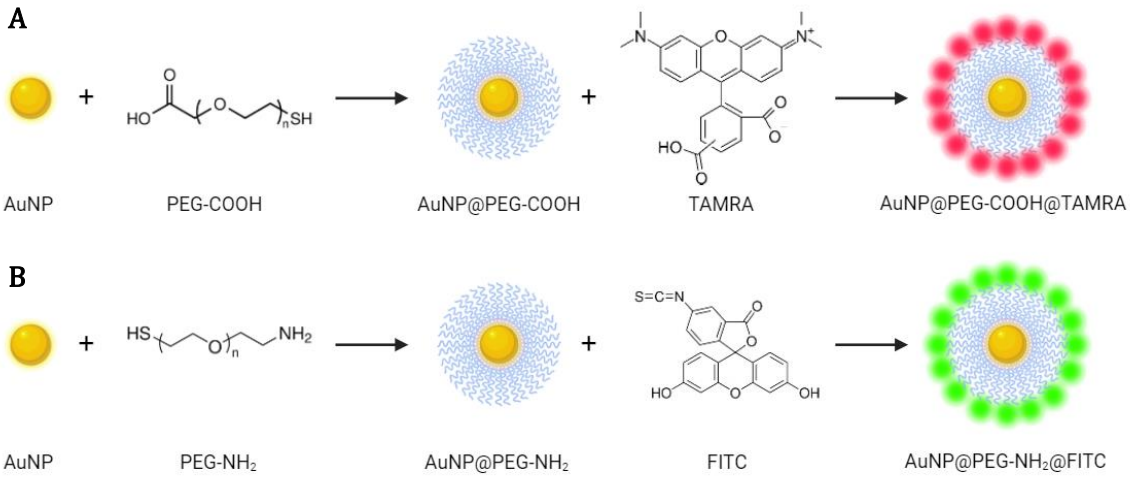

Figure 3.2 Schematic representation of the AuNPs functionalization reactions. **A** – AuNP@PEG-COOH@TAMRA. **B** – AuNP@PEG-NH_2@FITC.

3.2.1 Functionalization with PEG

In order to increase their stability and allow further functionalization with TAMRA and FITC, AuNPs were first functionalized with PEG-COOH and PEG-NH_2, respectively. The thiol groups present in both PEG chains present a high affinity to gold, and establish strong chemical bonds, thus replacing the existing weak adsorption bonds established by citrate, the previous capping agent. Therefore, the PEG molecules, substituted citrate, and formed an inert hydrophilic coating that inhibits the unwanted binding of other molecules[131].

Regarding the functionalization with PEG-COOH, AuNPs were coated with 30% surface coverage, resulting in a PEG concentration of 0.003 $mg.mL^{-1}$. The effectiveness of this functionalization was assessed by performing the Ellman's assys, quantifying the amount of free thiol groups in solution and, therefore, unbound PEG chains (Appendix A.1). After that, AuNPs were analysed by UV-Vis spectroscopy, which showed a minor redshift (approximately 2 nm) in the SPR peak, an indicator of a size increase in the AuNPs, resulting from the successful binding of PEG chains. There is also observable a slight increase in the SPR band, which can be related to an augment of the polydispersity (Figure 3.3).

Concerning the functionalization with PEG-NH_2, as mentioned, this protocol was optimized in the lab, in order to ensure maximum stability of AuNPs and functionalize them. In order to do so, 0.0025 g of PEG were added to $1x10^{-11}$ mol AuNPs. Again, AuNPs were analysed by UV-Vis spectroscopy. This time, the redshift was slightly bigger (4-6 nm), as the PEG-NH_2 chain is longer than the PEG-COOH, thus increasing the size of AuNPs even more. The SPR band was also enlarged (Figure 3.3).

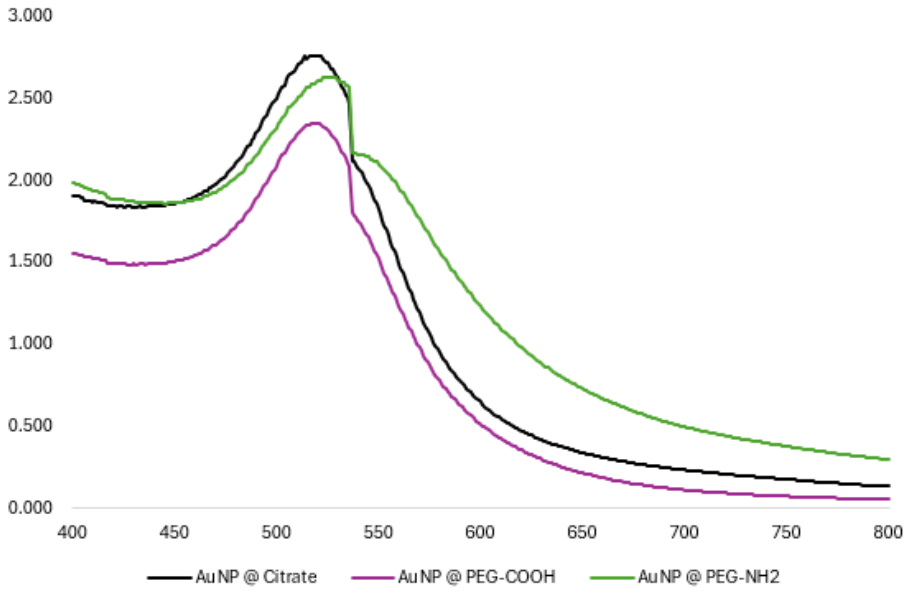

Figure 3.3 UV-Visible spectra of the functionalized AuNPs, for wavelengths ranging from 400-800 nm. Although there is a shift at 536 nm, the analysis of the SPR peaks can be done and are located at 522 nm for AuNP@PEG-COOH, and 525 nm for AuNP@PEG-NH_2.

3.2.2 Functionalization with TAMRA

After that, AuNP@PEG-COOH were further functionalized with TAMRA, a rhodamine-based fluorophore. The attachment of TAMRA allows the nanoconjugate to be observed with resource to fluorescence and was performed by an EDC/NHS coupled reaction. The amine groups present in the dye covalently bonded to the carboxyl groups of the PEG chains, resulting in AuNP@PEG-COOH@TAMRA.

Initially, the protocol used in Carreira (2015) was performed. This used a TAMRA concentration of 10^{-7} M. However, the resulting AuNPs did not possess measurable fluorescence (Figure 3.4, A). Therefore, the protocol needed to be adapted. Assuming that it could be a problem regarding the PEG chains. A new PEG sample was produced, using NaOH as a solvent, instead of H2O, in an attempt to increase the availability of the carboxyl groups in the PEG chains. However, this hypothesis was not confirmed as the resulting AuNPs still did not possess any fluorescence (Figure 3.4, B). Another hypothesis was then considered: the EDC and Sulfo-NHS samples were suspended in MES buffer, instead of being in aqueous conditions. This way, all of the reagents used in this functionalization were at the same pH value, minimizing the probability of a possible inhibition due to variations in the pH. Again, this hypothesis could not be confirmed, as the AuNPs still did not possess fluorescence (Figure 3.4, C).

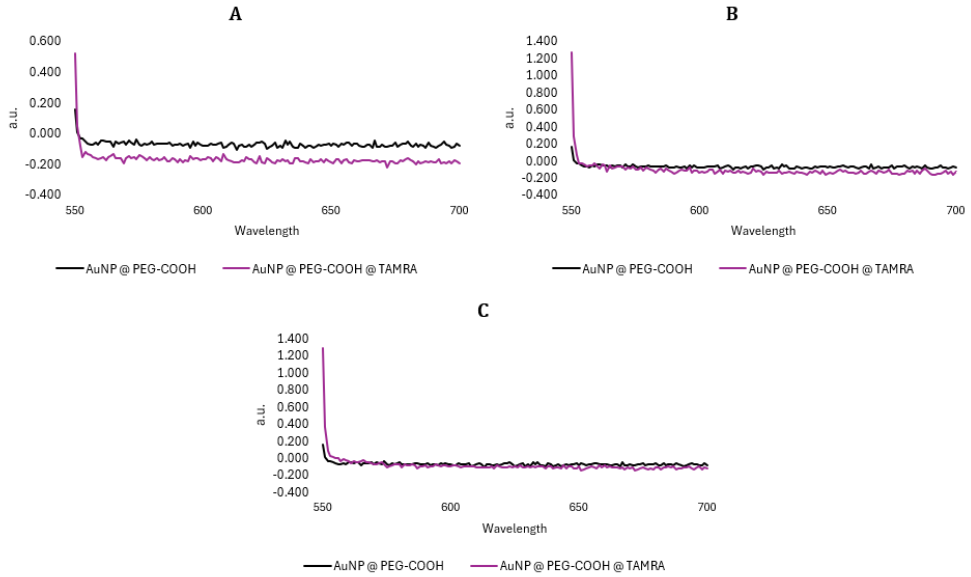

Figure 3.4 Emission spectra obtained for the functionalized AuNP@PEG-COOH@TAMRA, for wavelengths ranging from 550-700 nm, and with an excitation wavelength of 543 nm. **A –** Analysis of the AuNPs resulting from the original protocol; **B** – Analysis of the AuNPs obtained after the first adaptation (resuspending the PEG sample in NaOH); **C** – Analysis of the AuNPs obtained after the second adaptation to the protocol (resuspending EDC and Sulfo-NHS in MES buffer).

One final adaptation was made, and instead of using a TAMRA concentration of 10^{-7} M, TAMRA was added to the reactional system in a PEG:TAMRA ratio of 1:1.

The resulting nanoconjugate was characterized by UV-Visible spectroscopy, fluorescence spectroscopy and fluorescence microscopy. The amount of TAMRA dye bonded to the AuNPs was calculated by interpolating a calibration curve (Appendix A.2). The present SPR shift is minimal (1-2 nm) not being explicit by the observation of absorbance spectra, that present similar profiles Figure 3.5 A.

Fluorescence spectroscopy assays were conducted to assess the fluorescent properties of the nanoconjugate, with the fluorescence profile of AuNP@PEG-COOH@TAMRA present in Figure 3.5 B, indicating the bonding of the TAMRA molecule to the AuNP@PEG-COOH.

Finally, fluorescence microscopy was used to ensure that the fluorescence measured by spectroscopy was due to TAMRA molecules bound to the AuNPs and not to molecules dissolved in solution. Analysing the obtained images, depicted in Figure 3.5 C, it is possible to verify that most of the fluorescence signal comes from molecules bound to the AuNPs.

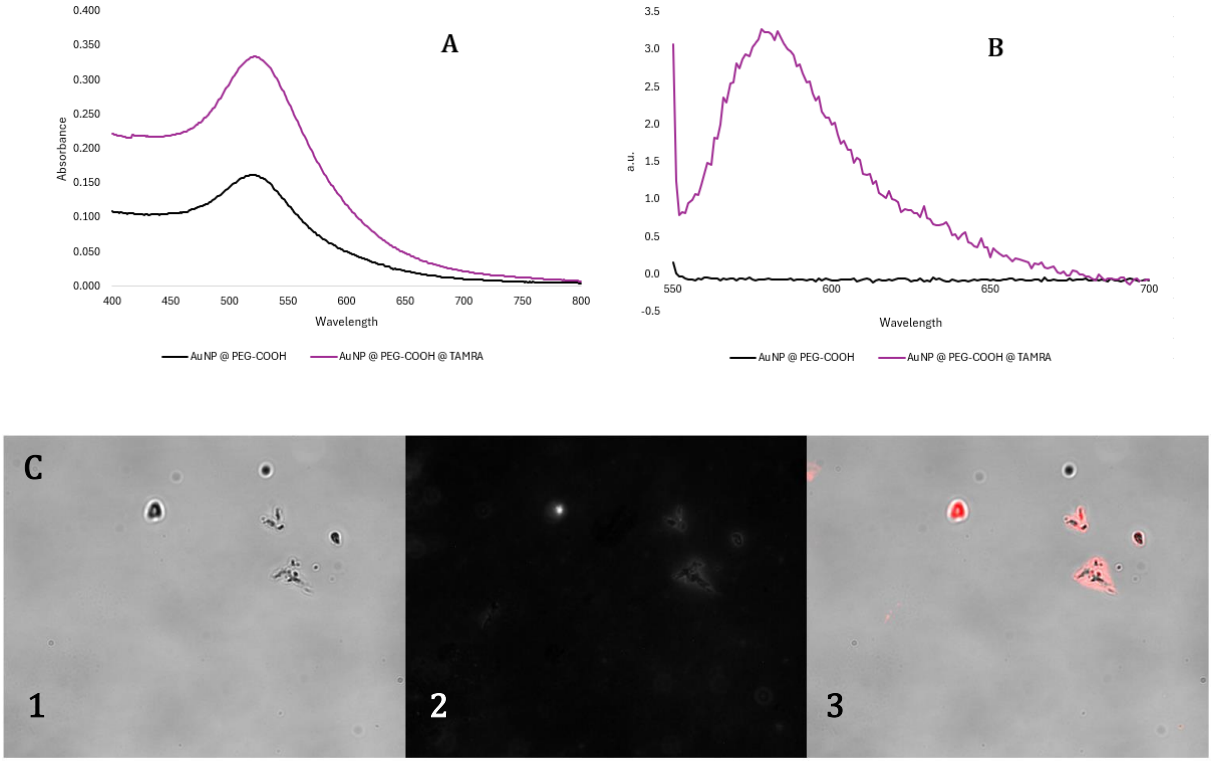

Figure 3.5 Characterization of the functionalized AuNP@PEG-COOH@TAMRA. **A** - UV-Visible absorption spectrum of the resulting AuNPs, compared to the previously functionalized AuNP@PEG-COOH. The SPR shift is no evident when looking at the spectra and the SPR band suffered minor alterations. **B** – Fluorescence Emission spectra obtained for the functionalized AuNPs, with an excitation wavelength of 543 nm. Contrary to the first results, AuNPs presented measurable fluorescence. **C** – Fluorescence Microscopy obtained for AuNP@PEG-COOH@TAMRA. 1) Bright field microscopy; 2) Fluorescence microscopy; 3) Integration of both images, to infer the provenience of the majority of the fluorescence signal. The fluorescence signal is mainly from TAMRA molecules bound to the AuNPs.

3.2.3 Functionalization with FITC

AuNP@PEG-NH_2 were functionalized with FITC, a green dye. The isothiocyanate group of the dye reacted to the amine groups of PEG chains, binding to the surface of AuNPs. AuNP@PEG-NH_2@FITC were also characterized via UV-Vis spectroscopy, fluorescence spectroscopy and fluorescence microscopy. The amount of FITC bonded to the AuNPs was calculated by interpolating a calibration curve (Appendix A.3). UV-Vis spectroscopy shows that, once again, the addition of the dye did not induce a significant redshift on the system, nor an enlargement of the SPR band, meaning that, similarly to the AuNP@PEG-COOH@TAMRA, the AuNPs' diameter and monodispersity remained practically the same (Figure 3.6 A).

The fluorescence profile of AuNP@PEG-NH_2@FITC was also assessed by fluorescence spectroscopy, with the results present in Figure 3.6 B. The fluorescence intensity of FITC is not very high, probably because of the internal shielding effect that AuNPs can perform.

Once again, in order to ensure that the fluorescence measured by spectroscopy was due to FITC molecules bound to the AuNPs and not to molecules dissolved in solution, AuNPs were analysed

by fluorescence microscopy. Analysing the obtained images, it is possible to verify that most of the fluorescence signal comes from molecules bound to the AuNPs (Figure 3.6 C)

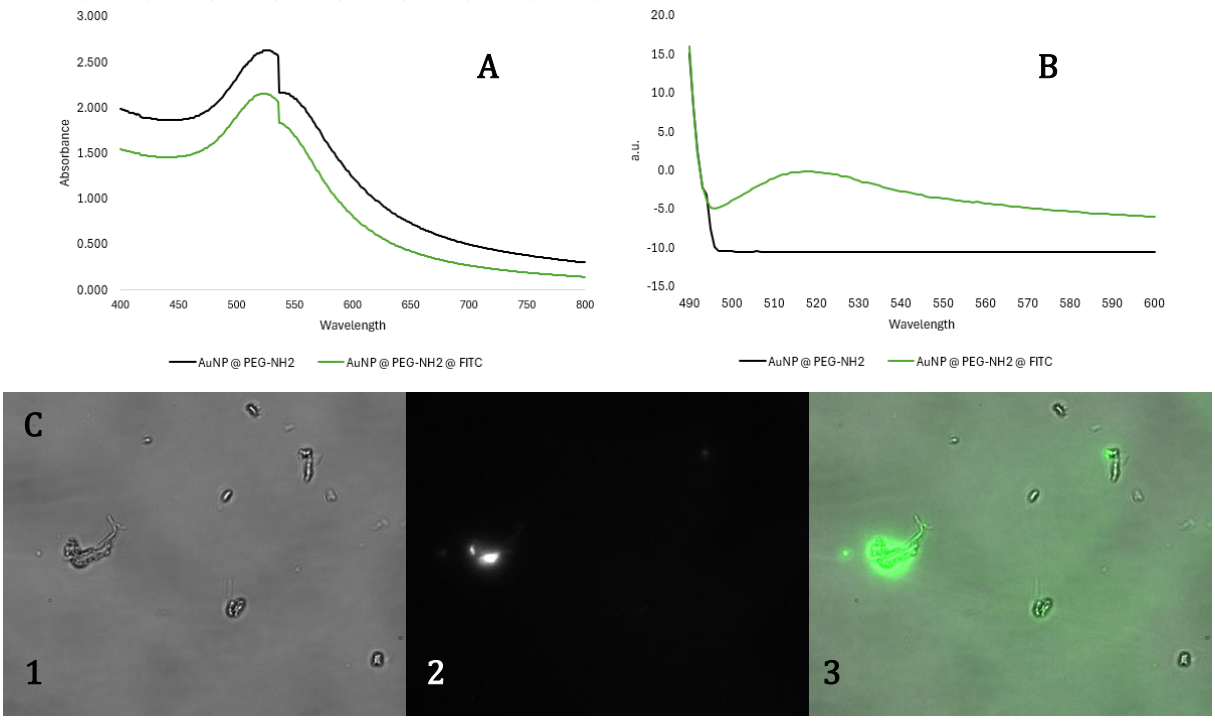

Figure 3.6 Characterization of the functionalized AuNP@PEG-NH_2@FITC. **A** – UV-Visible absorption spectrum, compared to the previously synthesised AuNP@PEG-NH_2. Although there is an absorbance shift at 536 nm, both curves are similar, and the SPR band and its maximum did not change. **B** – Fluorescence emission spectrum of the AuNP@PEG-NH_2@FITC, for wavelengths ranging from 490-600 nm, with an excitation wavelength of 488 nm. **C** – Fluorescence Microscopy obtained for AuNP@PEG-NH_2@FITC. 1) Bright field microscopy; 2) Fluorescence microscopy; 3) Integration of both images, to infer the provenience of the majority of the fluorescence signal. Although there is the presence of signal in the medium, the fluorescence signal is mainly from FITC molecules bound to the AuNPs.

3.3 pH Stability Assessment

One of the initial objectives of this project was to study the possibility of functionalizing AuNPs with both fluorescent dyes. For that, phosphate buffer saline (PBS) with different pH values (5, 6, 7, 8) was used. PBS is a widely used buffer for biomedical applications. The presence of salt changes the dielectric constant of the medium, being an instability factor for AuNPs[53].

10 nM AuNPs were resuspended in each condition and absorbance and fluorimetry readings were obtained at the selected time points (2, 4, 6 hours). Realizing a macroscopic analysis (Appendix A.4) of the samples it was possible to see that the AuNP@PEG-COOH@TAMRA samples at pH 5 and 6 completely decharacterized. The samples lost their unique and characteristic reddish colour, probably due to changes in the ionic strength of the medium, leading to aggregation of AuNPs.

3.3.1 AuNP@PEG-COOH@TAMRA

3.3.1.1 UV-Visible Spectroscopy

As mentioned, these AuNPs were highly unstable at pH 5 and 6. This supposition can be corroborated by the analysis of the absorbance spectra. For pH 5, the SPR peak diminishes over time, a considerable redshift occurs and the SPR band is highly enlarged. These are all indicators of instability in the nanoconjugates, as the AuNP concentration decreases, and they become more and more polydisperse. At pH 6, the curves were less decharacterized. The intensity of the SPR peaks suffered less variations over time, the redshift was smaller and the SPR band did not enlarge that much. However, AuNPs were still too unstable (Figure 3.7).

At pH 7, the profile of the curves were all similar, with several less variation of the SPR peaks and enlargement of the SPR band. As for pH 8, the curves overlapped each other, being almost coincident. In these conditions there were observable the less changes in the normal behaviour of AuNPs (Figure 3.7).

Changing the suspension buffer (AuNPs were functionalized in MES buffer, and the pH stability assays were conducted in PBS 1x) can influence the ionic strength of the solution, influencing AuNP stability. At acidic pH, the ionic strength is enhanced, which could lead to the protonation of the carboxyl groups in the PEG molecule, decreasing the negative charge on the AuNPs' surface, thus leading to a reduction in the electrostatic repulsions between AuNPs, promoting aggregation[132].

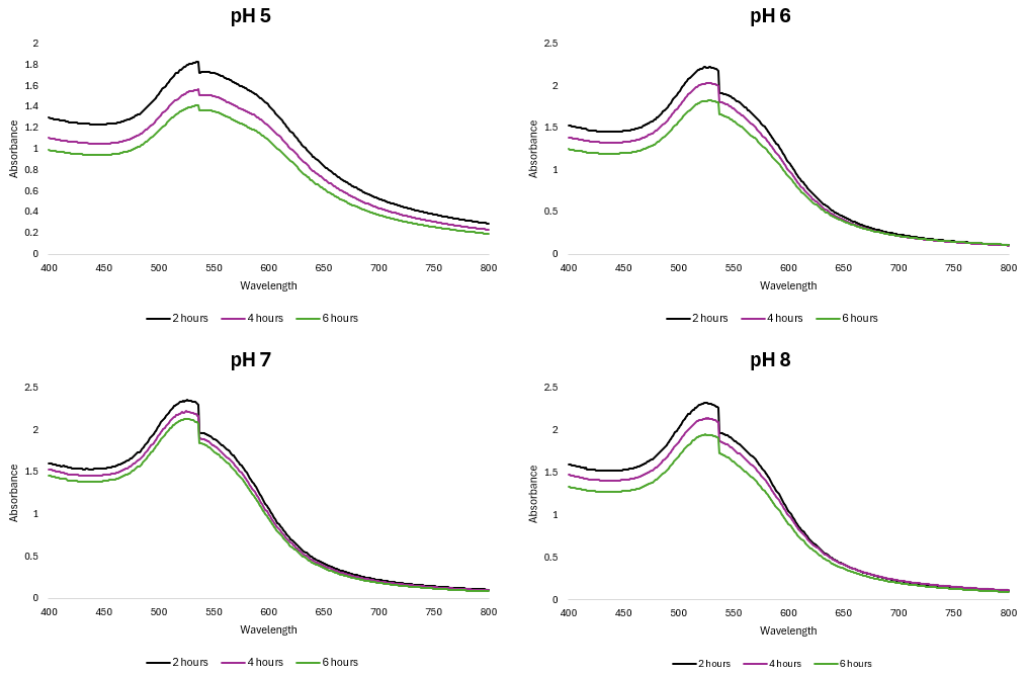

Figure 3.7 UV-Visible absorption spectrum for AuNP@PEG-COOH@TAMRA, for each condition**.** For pH 5, there was a large broadening of the SPR band, as well as a redshift at its peak. pH 7 was the condition that less impacted the stability of the nanoconjugate, with very similar profiles over time.

3.3.1.2 Fluorescence Spectroscopy

The TAMRA molecule is not pH-sensitive, as its properties do not change with variations of pH[112,113]. Therefore, changes on the fluorescence intensity of the AuNP@PEG-COOH@TAMRA samples were not expected. However, that was not the case. Although not varying over time, the intensity of the fluorescence peak decreased with the increase in pH values (Figure 3.8). This can be due to the increasing stability of the AuNPs. AuNPs can act as internal shields, preventing the fluorescence to be detected by the sensor. When AuNPs destabilise, they tend to aggregate, losing the optical properties already mentioned. Additionally, when functionalised with TAMRA, the dye's molecules will unbind from the AuNPs, and they will aggregate forming larger clusters. This will reduce the number of particles in solution, also reducing the number of "shields", allowing for the excitation of a higher number of TAMRA molecules, which leads to a higher number of TAMRA molecules emitting fluorescence and, therefore, an increase in the detection of fluorescence[133].

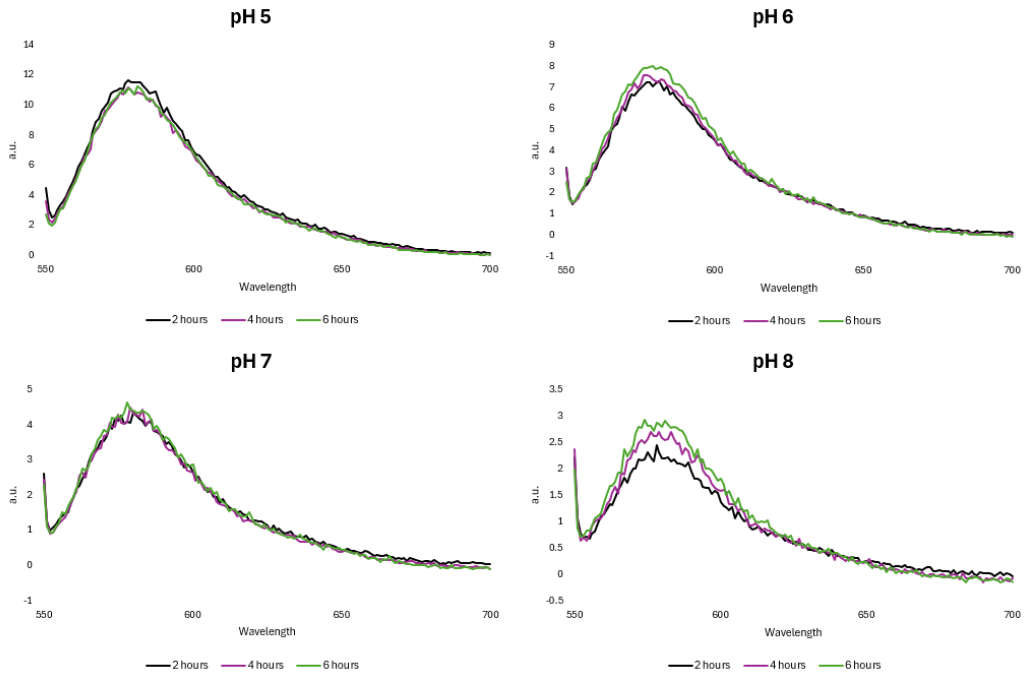

Figure 3.8 Fluorescence emission spectra of AuNP@PEG-COOH@TAMRA, for each condition. Although the signal is stable overtime, it decreases as the pH increases.

3.3.2 AuNP@PEG-NH_2@FITC

3.3.2.1 UV-Visible Spectroscopy

In every condition, the curve's profile did not change. The SPR peak remained the same and did not redshift, thus indicating that the concentration of viable AuNPs did not change significantly. The SPR band also did not change, indicating that the AuNPs remained monodisperse and stable (Figure 3.9). In fact, in all conditions, the curves overlapped in the two first time points, with a slight decrease at 6 hours.

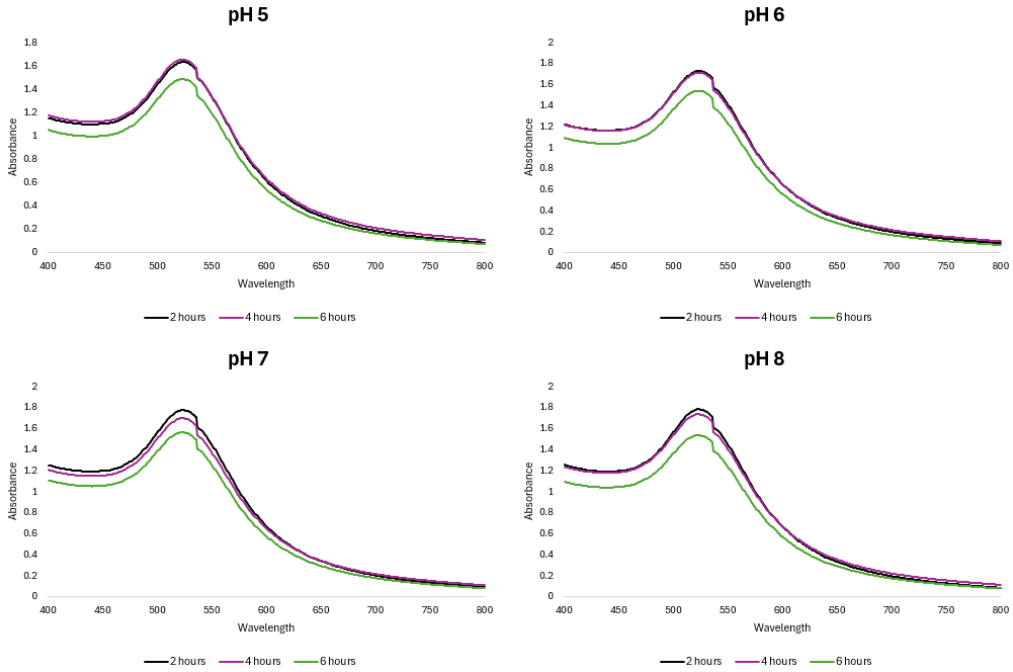

Figure 3.9 UV-Visible absorption spectrum for AuNP@PEG-NH_2@FITC, for each condition. In all samples, the obtained curves were similar, with a small intensity decrease at 6 hours. The SPR bands and peaks did not change over time, or condition.

3.3.2.2 Fluorescence Spectroscopy

According to the literature, FITC is pH sensitive[114–116], being used as an indicator, when conjugated with nanoparticles, in pH-dependent drug delivery studies. Its relative fluorescence increases with the increase of pH. This is observable when analysing the fluorescence spectra obtained (Figure 3.10). Although it is not evident while analysing the spectra, due to the low intensity of the fluorescence signal, this increase is present (Table 3.1). The values of the fluorescence intensity of the nanoconjugates, in the following table, confirm that increase in fluorescence. Being a pH-sensitive fluorescent dye, FITC's properties are affected by the protonation or deprotonation of its fluorescein moiety. At acidic pH, FITC is protonated, quenching its fluorescence. As the pH increases, the resulting deprotonation of the FITC molecule leads to a more efficient electronic transition, enhancing its fluorescence intensity [114–116].

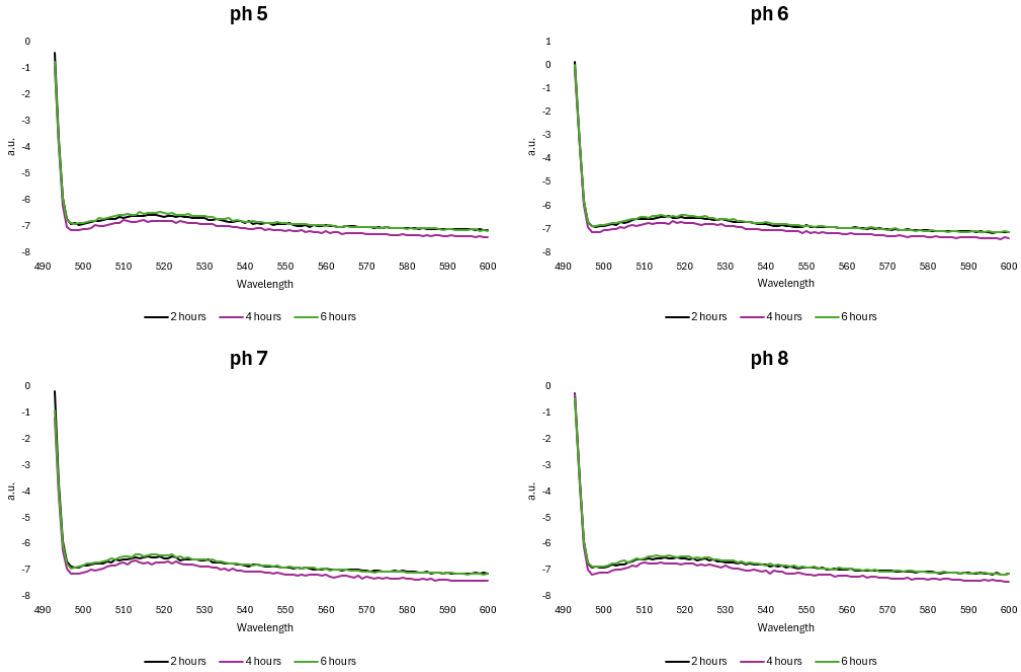

Figure 3.10 Fluorescence emission spectra of AuNP@PEG-NH_2@FITC, for each condition**.** All samples presented similar curves. However, there is a slight fluoresce intensity increase, as the pH increases.

Table 3.1 — Values of the intensity peaks of the fluorescence spectroscopy assays. Although not evident analyzing the spectra, the intensity of the fluorescence increased with the increase in pH, due to the protonation of the FITC molecule, which led to a decrease in fluorescent intensity, at lower pH.

	pH 5	pH 6	pH 7	pH 8
2 hours	-6.67	-6.64	-6.64	-6.51
4 hours	-6.78	-6.69	-6.66	-6.53
6 hours	-6.67	-6.67	-6.48	-6.43
Mean	-6.71	-6.67	-6.59	-6.49

3.3.3 AuNPs Concentration

In order to better understand the effect of pH in the AuNPs, calculations on their concentration were conducted. However, absolute values are not considered, being considered only the variation over time and pH.

Regarding AuNP@PEG-COOH@TAMRA, as expected due to what was previously studied, for pH 5 and 6, AuNP concentration decreased significantly, with only 36.13% and 39.63% of functional AuNPs, after 6 hours (Figure 3.11). However, for pH 7 (84.60%) and 8 (80.10%) the decrease was not so drastic over the 6 hours, being similar between the two conditions.

For the AuNP@PEG-NH_2@FITC, the variation of the concentration of AuNPs was practically constant amongst all conditions and timepoints. Only the sample at pH 5 did not present a percentage of functional AuNPs over 80% (79.50%) (Figure 3.11).

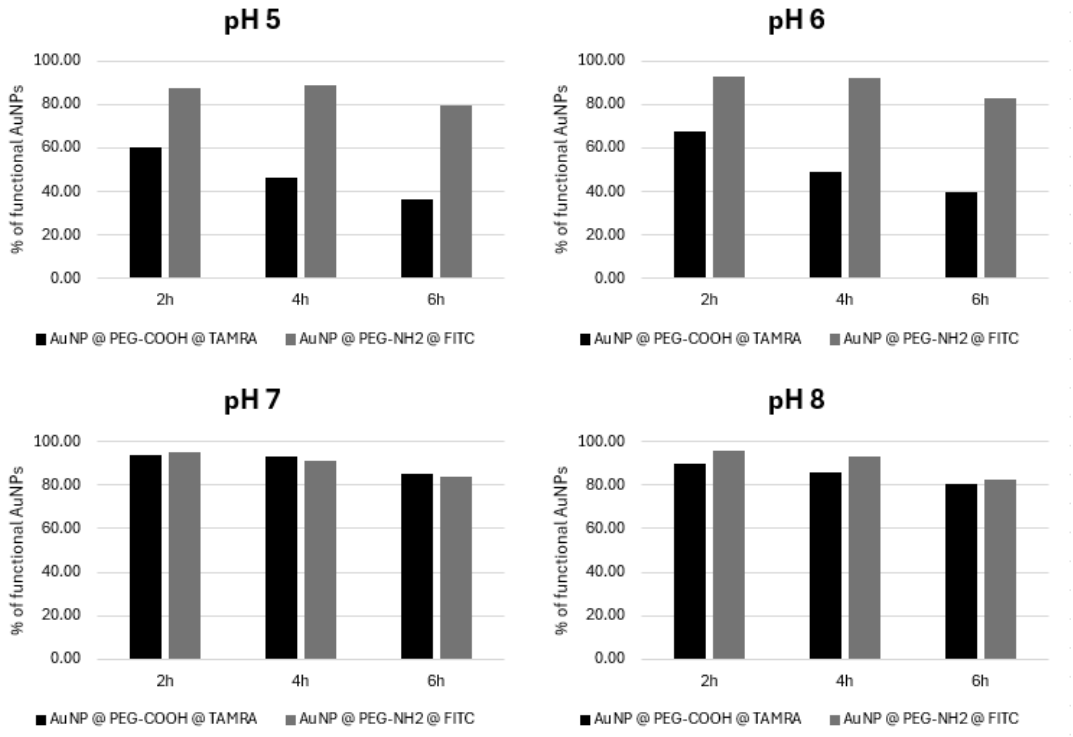

Figure 3.11 Percentage of functional AuNPs in each sample, for every condition. pH 7 was the condition that allowed for AuNPs with the better stability, having the higher percentage of functional AuNPs.

3.3.4 Absorbance Maxima

Since the AuNPs presented different degrees of stability, macroscopically, the SPR peaks of each sample were analysed to infer if there were any considerable deviations in the monodispersity and colloidal stability of the AuNPs. Prior to these assays, the absorbance SPR peaks were at 523 nm for AuNP@PEG-COOH@TAMRA and 522 nm for AuNP@PEG-NH_2@FITC. Figure 3.12 incorporates the wavelength variation where the absorption was maximal, for all conditions, at every timepoint. As mentioned earlier, the absorbance spectra of AuNP@PEG-COOH@TAMRA presented a severe redshift at pH 5, that was gradually reducing as pH increased. This information is corroborated by the analysis of the SPR peak for each condition, where the values for pH 5 are extremely higher than the initial 524 nm, but for pH 8, these values are more similar to them. For AuNP@PEG-NH_2@FITC, the obtained values are not much different from the initial 522 nm (Figure 3.12).

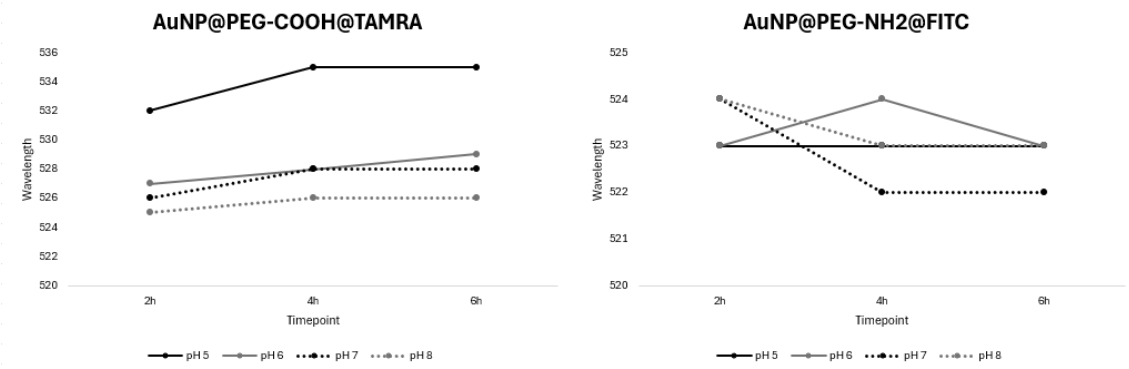

Figure 3.12 Variation of the SPR peaks for each type of AuNP. AuNP@PEG-COOH@TAMRA were highly affected at pH 5, with a considerable redshift at pH 6 also. AuNP@PEG-NH_2@FITC were more stable, with the redshift varying from 1-2 nm)

Overall, AuNP@PEG-NH_2@FITC are less susceptible to the effect of pH than AuNP@PEG-COOH@TAMRA. Given the showed results, for a possible functionalization of AuNPs with both dyes, the AuNPs should be functionalized and stored at pH 7, for minimal destabilization of AuNPs, while maintaining the interesting properties of TAMRA and FITC.

As previously mentioned, due to personal constraints, this work could only be performed to this extent. However, if the fluorescent probes could be designed and tested in cancer cells, they were going to be, theoretically, good trackers of the intracellular fate of AuNPs. Interpolating the experimental results, it is possible to infer that, in the acidic environment of endocytic vesicles, the relative fluorescence of both TAMRA and FITC would vary through the pathway. The double-functionalized AuNPs would be more stable than AuNP@PEG-COOH@TAMRA, thus not aggregating so much in acidic environments. Yet, the carboxyl groups in the PEG chains would still be protonated and an increase in the fluorescence signal of TAMRA would be expected. On the other hand, the fluorescein moiety of FITC would be protonated in those environments, thus quenching the emission of fluorescence by this fluorophore, reducing the fluorescence intensity of FITC.

4

Conclusion and Future Perspectives

Cancer is still one of the major causes of mortality in the entire world. Conventional therapies often lack selectivity and specificity. Because of this, nanomedicine is emerging with innovative methods for therapy and diagnostics. In this work, the initial objective was to successfully functionalise AuNPs with TAMRA and FITC, allowing the track of their intracellular fate. However, due to personal and familiar reasons these could not be achieved and were readapted.

AuNPs were synthesized by the citrate-reduction method, and analysed by UV-Vis spectroscopy, where a symmetric SPR peak at 519 nm. After that, AuNPs were functionalized with two distinct PEG molecules, and then characterized by UV-Vis spectroscopy, with maximal absorbance readings at 522 and 525 nm for AuNP@PEG-COOH and AuNP@PEG-NH_2, respectively. After that, AuNPs were furtherly functionalised with two fluorescent dyes (TAMRA and FITC) and were characterized by UV-Vis spectroscopy, fluorescence spectroscopy and fluorescence microscopy. This time, the SPR band remained the same, with minimal changes.

The effect of pH was then tested, in order to infer whether or not the AuNPs were stable in different conditions and decide the working pH for the double functionalisation. AuNP@PEG-NH_2@FITC were found to be less susceptible to the effect of pH than AuNP@PEG-COOH@TAMRA, as they presented less changes in the stability of the samples. At lower pH values, AuNP@PEG-COOH@TAMRA highly aggregated, possibly due to protonation of carboxyl groups in the PEG chain. The fluorescent intensity of TAMRA diminished, as the pH increased, which could be explained by the aggregation of AuNPs, reducing the influence of the "shielding" effect. However, AuNP@PEG-NH_2@FITC slightly increased its fluorescent intensity, as the FITC molecules became less protonated, reducing the fluorescence quenching effect. Given the experimental results, the pH that better allowed the functionalisation of both dyes, while maintaining the properties of both dyes, was 7.

The greatest set back of this work, besides the ones already mentioned, was the TAMRA functionalisation. For about 1 month, TAMRA functionalised AuNPs presented no fluorescence, and so several protocol adaptations were conducted, until the fluorescence signal was significant.

Although the experimental work did not proceed to its predicted full extent, these results show that the design of AuNP-based probes for the tracking of the intracellular fate of AuNPs has an interesting future, as the intravesicular environment becomes more acidic as the endocytic pathway progresses.

This work is neither the beginning nor the end. It is a part of a long journey, and in the future, if the functionalization of a single AuNP with both dyes becomes possible, it will open up significant opportunities in the field of nanomedicine.

REFERENCES

1. McGuire, S. World Cancer Report 2014. Geneva, Switzerland: World Health Organization, International Agency for Research on Cancer, WHO Press, 2015. *Advances in Nutrition* **7**, 418–419 (2016).
2. Siegel, R. L., Miller, K. D. & Jemal, A. Cancer statistics, 2018. *CA Cancer J Clin* **68**, 7–30 (2018).
3. Conde, J. The Golden Age in Cancer Nanobiotechnology: Quo Vadis? *Front Bioeng Biotechnol* **3**, (2015).
4. Ferlay J *et al.* Global Cancer Observatory: Cancer Today. *International Agency for Research on Cancer* https://gco.iarc.who.int/today (2024).
5. Cai, W. Applications of gold nanoparticles in cancer nanotechnology. *Nanotechnol Sci Appl* **Volume 1**, 17–32 (2008).
6. Eustis, S. & El-Sayed, M. A. Why gold nanoparticles are more precious than pretty gold: Noble metal surface plasmon resonance and its enhancement of the radiative and nonradiative properties of nanocrystals of different shapes. *Chem. Soc. Rev.* **35**, 209–217 (2006).
7. Reddy, V. R. Gold nanoparticles: Synthesis and applications. *Synlett* 1791–1792 (2006) doi:10.1055/s-2006-944219.
8. Bhattacharyya, D., Singh, S., Satnalika, N., Khandelwal, A. & Jeon, S.-H. *Nanotechnology, Big Things from a Tiny World: A Review*. *International Journal of u-and e-Service* vol. 2 (2009).
9. Chithrani, B. D., Ghazani, A. A. & Chan, W. C. W. Determining the Size and Shape Dependence of Gold Nanoparticle Uptake into Mammalian Cells. *Nano Lett* **6**, 662–668 (2006).
10. Conde, J. *et al.* Revisiting 30 years of biofunctionalization and surface chemistry of inorganic nanoparticles for nanomedicine. *Front Chem* **2**, (2014).
11. Heath, J. R. & Davis, M. E. Nanotechnology and Cancer. *Annu Rev Med* **59**, 251–265 (2008).
12. Sperling, R. A., Rivera Gil, P., Zhang, F., Zanella, M. & Parak, W. J. Biological applications of gold nanoparticles. *Chem Soc Rev* **37**, 1896 (2008).
13. Salata, O. Applications of nanoparticles in biology and medicine. *J Nanobiotechnology* **2**, 3 (2004).
14. Jain, K. K. Nanomedicine: Application of Nanobiotechnology in Medical Practice. *Medical Principles and Practice* **17**, 89–101 (2008).

15. Sahay, G., Alakhova, D. Y. & Kabanov, A. V. Endocytosis of nanomedicines. *Journal of Controlled Release* **145**, 182–195 (2010).
16. Cai, W. *et al.* Peptide-Labeled Near-Infrared Quantum Dots for Imaging Tumor Vasculature in Living Subjects. *Nano Lett* **6**, 669–676 (2006).
17. Park, J. W., Benz, C. C. & Martin, F. J. Future directions of liposome- and immunoliposome-based cancer therapeutics. *Semin Oncol* **31**, 196–205 (2004).
18. Huang, X., Jain, P. K., El-Sayed, I. H. & El-Sayed, M. A. Gold nanoparticles: interesting optical properties and recent applications in cancer diagnostics and therapy. *Nanomedicine* **2**, 681–693 (2007).
19. Pitkethly, M. J. Nanomaterials – the driving force. *Materials Today* **7**, 20–29 (2004).
20. Liu, Z. *et al.* In vivo biodistribution and highly efficient tumour targeting of carbon nanotubes in mice. *Nat Nanotechnol* **2**, 47–52 (2007).
21. Boisselier, E. & Astruc, D. Gold nanoparticles in nanomedicine: preparations, imaging, diagnostics, therapies and toxicity. *Chem Soc Rev* **38**, 1759 (2009).
22. Lammers, T., Aime, S., Hennink, W. E., Storm, G. & Kiessling, F. Theranostic Nanomedicine. *Acc Chem Res* **44**, 1029–1038 (2011).
23. Cai, W., Hsu, A. R., Li, Z.-B. & Chen, X. Are quantum dots ready for in vivo imaging in human subjects? *Nanoscale Res Lett* **2**, 265 (2007).
24. Bozzuto, G. & Molinari, A. Liposomes as nanomedical devices. *Int J Nanomedicine* 975 (2015) doi:10.2147/IJN.S68861.
25. Dai, H. Carbon nanotubes: opportunities and challenges. *Surf Sci* **500**, 218–241 (2002).
26. Sadegh, H. & Ghoshekandi, R. S. Functionalization of Carbon Nanotubes and its Application in Nanomedicine: A Review. *Nanomed J* **2**, 231–248 (2015).
27. Burygin, G. *et al.* On the Enhanced Antibacterial Activity of Antibiotics Mixed with Gold Nanoparticles. *Nanoscale Res Lett* **4**, 794 (2009).
28. Mody, V., Siwale, R., Singh, A. & Mody, H. Introduction to metallic nanoparticles. *J Pharm Bioallied Sci* **2**, 282 (2010).
29. Kumar, H., Venkatesh, N., Bhowmik, H. & Kuila, A. Metallic Nanoparticle: A Review. *Biomed J Sci Tech Res* **4**, 3765–3775 (2018).
30. Awan, I., Hussain, S., Haq, A. & Khan, A. Wondrous Nanotechnology. *Journal of the Chemical Society of Pakistan* **38**, 1026–1055 (2016).
31. Mieszawska, A. J., Mulder, W. J. M., Fayad, Z. A. & Cormode, D. P. Multifunctional Gold Nanoparticles for Diagnosis and Therapy of Disease. *Mol Pharm* **10**, 831–847 (2013).
32. Baptista, P. *et al.* Gold nanoparticles for the development of clinical diagnosis methods. *Anal Bioanal Chem* **391**, 943–950 (2008).
33. Vigderman, L. & Zubarev, E. R. Therapeutic platforms based on gold nanoparticles and their covalent conjugates with drug molecules. *Adv Drug Deliv Rev* **65**, 663–676 (2013).

34. Huang, X., Jain, P. K., El-Sayed, I. H. & El-Sayed, M. A. Plasmonic photothermal therapy (PPTT) using gold nanoparticles. *Lasers Med Sci* **23**, 217–228 (2008).
35. Cordeiro, M., Ferreira Carlos, F., Pedrosa, P., Lopez, A. & Baptista, P. Gold Nanoparticles for Diagnostics: Advances towards Points of Care. *Diagnostics* **6**, 43 (2016).
36. Abadeer, N. & Murphy, C. *Nanomaterials and Neoplasms*. (Jenny Stanford Publishing, 2021). doi:10.1201/9780429027819.
37. Jain, P. K., Lee, K. S., El-Sayed, I. H. & El-Sayed, M. A. Calculated Absorption and Scattering Properties of Gold Nanoparticles of Different Size, Shape, and Composition: Applications in Biological Imaging and Biomedicine. *J Phys Chem B* **110**, 7238–7248 (2006).
38. Huang, X. & El-Sayed, M. A. Gold nanoparticles: Optical properties and implementations in cancer diagnosis and photothermal therapy. *J Adv Res* **1**, 13–28 (2010).
39. Larguinho, M. *et al.* Gold nanoprobe-based non-crosslinking hybridization for molecular diagnostics. *Expert Rev Mol Diagn* **15**, 1355–1368 (2015).
40. Collado-González, M. *et al.* Aggregation behaviour of gold nanoparticles in presence of chitosan. *Journal of Nanoparticle Research* **17**, 268 (2015).
41. Sun, Y. & Xia, Y. Shape-Controlled Synthesis of Gold and Silver Nanoparticles. *Science (1979)* **298**, 2176–2179 (2002).
42. El-Brolossy, T. A. *et al.* Shape and size dependence of the surface plasmon resonance of gold nanoparticles studied by Photoacoustic technique. *Eur Phys J Spec Top* **153**, 361–364 (2008).
43. Tiwari, P., Vig, K., Dennis, V. & Singh, S. Functionalized Gold Nanoparticles and Their Biomedical Applications. *Nanomaterials* **1**, 31–63 (2011).
44. Huang, X. & El-Sayed, M. A. Plasmonic photo-thermal therapy (PPTT). *Alexandria Journal of Medicine* **47**, 1–9 (2011).
45. Low, A. & Bansal, V. A visual tutorial on the synthesis of gold nanoparticles. *Biomed Imaging Interv J* **6**, (2010).
46. John Turkevich, B., Cooper Stevenson, P. & Hillier, J. *A STUDY OF THE NUCLEATION AND GROWTH PROCESSES I N THE SYNTHESIS OF COLLOIDAL GOLD*. *Anal. Chem* vol. 47 (1941).
47. Love, J. C., Estroff, L. A., Kriebel, J. K., Nuzzo, R. G. & Whitesides, G. M. Self-Assembled Monolayers of Thiolates on Metals as a Form of Nanotechnology. *Chem Rev* **105**, 1103–1170 (2005).
48. Bastús, N. G., Comenge, J. & Puntes, V. Kinetically Controlled Seeded Growth Synthesis of Citrate-Stabilized Gold Nanoparticles of up to 200 nm: Size Focusing versus Ostwald Ripening. *Langmuir* **27**, 11098–11105 (2011).
49. DeLong, R., Dr. Adam Wanekaya, Mr. Chris Reynolds & Schaeffer, A. Functionalized gold nanoparticles for the binding, stabilization, and delivery of therapeutic DNA, RNA, and

other biological macromolecules. *Nanotechnol Sci Appl* 53 (2010) doi:10.2147/NSA.S8984.

50. Thanh, N. T. K. & Green, L. A. W. Functionalisation of nanoparticles for biomedical applications. *Nano Today* **5**, 213–230 (2010).
51. Doria, G. *et al.* Noble Metal Nanoparticles for Biosensing Applications. *Sensors* **12**, 1657–1687 (2012).
52. Manson, J., Kumar, D., Meenan, B. J. & Dixon, D. Polyethylene glycol functionalized gold nanoparticles: the influence of capping density on stability in various media. *Gold Bull* **44**, 99–105 (2011).
53. Jokerst, J. V, Lobovkina, T., Zare, R. N. & Gambhir, S. S. Nanoparticle PEGylation for imaging and therapy. *Nanomedicine* **6**, 715–728 (2011).
54. OWENSIII, D. & PEPPAS, N. Opsonization, biodistribution, and pharmacokinetics of polymeric nanoparticles. *Int J Pharm* **307**, 93–102 (2006).
55. Dreaden, E. C., Alkilany, A. M., Huang, X., Murphy, C. J. & El-Sayed, M. A. The golden age: gold nanoparticles for biomedicine. *Chem. Soc. Rev.* **41**, 2740–2779 (2012).
56. Grabarek, Z. & Gergely, J. Zero-length crosslinking procedure with the use of active esters. *Anal Biochem* **185**, 131–135 (1990).
57. Conde, J. *et al.* Design of Multifunctional Gold Nanoparticles for *In Vitro* and *In Vivo* Gene Silencing. *ACS Nano* **6**, 8316–8324 (2012).
58. Chen, C. & Hildebrandt, N. Resonance energy transfer to gold nanoparticles: NSET defeats FRET. *TrAC Trends in Analytical Chemistry* **123**, 115748 (2020).
59. Chen, C., Midelet, C., Bhuckory, S., Hildebrandt, N. & Werts, M. H. V. Nanosurface Energy Transfer from Long-Lifetime Terbium Donors to Gold Nanoparticles. *The Journal of Physical Chemistry C* **122**, 17566–17574 (2018).
60. Jeong, E. H., Jung, G., Hong, C. A. & Lee, H. Gold nanoparticle (AuNP)-based drug delivery and molecular imaging for biomedical applications. *Archives of Pharmacal Research* vol. 37 53–59 Preprint at https://doi.org/10.1007/s12272-013-0273-5 (2014).
61. Lee, H., Lee, K., Kim, I. & Park, T. G. Fluorescent Gold Nanoprobe Sensitive to Intracellular Reactive Oxygen Species. *Adv Funct Mater* **19**, 1884–1890 (2009).
62. Bunz, U. H. F. & Rotello, V. M. Gold Nanoparticle–Fluorophore Complexes: Sensitive and Discerning "Noses" for Biosystems Sensing. *Angewandte Chemie International Edition* **49**, 3268–3279 (2010).
63. Cabral, R. M. & Baptista, P. V. Anti-cancer precision theranostics: a focus on multifunctional gold nanoparticles. *Expert Rev Mol Diagn* **14**, 1041–1052 (2014).
64. Baptista, P. *et al.* Gold nanoparticle-based theranostics: disease diagnostics and treatment using a single nanomaterial. *Nanobiosensors in Disease Diagnosis* 11 (2015) doi:10.2147/NDD.S60285.

65. Xu, Z. P., Zeng, Q. H., Lu, G. Q. & Yu, A. B. Inorganic nanoparticles as carriers for efficient cellular delivery. *Chem Eng Sci* **61**, 1027–1040 (2006).
66. Bouché, M. *et al.* Recent Advances in Molecular Imaging with Gold Nanoparticles. *Bioconjug Chem* **31**, 303–314 (2020).
67. Cho, E. C., Glaus, C., Chen, J., Welch, M. J. & Xia, Y. Inorganic nanoparticle-based contrast agents for molecular imaging. *Trends Mol Med* **16**, 561–573 (2010).
68. Wu, Y., Ali, M. R. K., Chen, K., Fang, N. & El-Sayed, M. A. Gold nanoparticles in biological optical imaging. *Nano Today* vol. 24 120–140 Preprint at https://doi.org/10.1016/j.nantod.2018.12.006 (2019).
69. Lee, H., Lee, K., Kim, I. K. & Park, T. G. Synthesis, characterization, and in vivo diagnostic applications of hyaluronic acid immobilized gold nanoprobes. *Biomaterials* **29**, 4709–4718 (2008).
70. Kim, D., Jeong, Y. Y. & Jon, S. A Drug-Loaded Aptamer—Gold Nanoparticle Bioconjugate for Combined CT Imaging and Therapy of Prostate Cancer. *ACS Nano* **4**, 3689–3696 (2010).
71. Cole, L. E., Ross, R. D., Tilley, J. M., Vargo-Gogola, T. & Roeder, R. K. Gold nanoparticles as contrast agents in X-ray imaging and computed tomography. *Nanomedicine* vol. 10 321–341 Preprint at https://doi.org/10.2217/nnm.14.171 (2015).
72. Shilo, M., Reuveni, T., Motiei, M. & Popovtzer, R. Nanoparticles as Computed Tomography Contrast Agents: Current Status and Future Perspectives. *Nanomedicine* **7**, 257–269 (2012).
73. Jakhmola, A., Anton, N. & Vandamme, T. F. Inorganic Nanoparticles Based Contrast Agents for X-ray Computed Tomography. *Adv Healthc Mater* **1**, 413–431 (2012).
74. Brannon-Peppas, L. & Blanchette, J. O. Nanoparticle and targeted systems for cancer therapy. *Adv Drug Deliv Rev* **56**, 1649–1659 (2004).
75. Brigger, I., Dubernet, C. & Couvreur, P. Nanoparticles in cancer therapy and diagnosis. *Adv Drug Deliv Rev* **64**, 24–36 (2012).
76. Li, W. & Chen, X. Gold nanoparticles for photoacoustic imaging. *Nanomedicine* vol. 10 299–320 Preprint at https://doi.org/10.2217/nnm.14.169 (2015).
77. Kavalaraki, A., Spyratou, E., Kouri, M. A. & Efstathopoulos, E. P. Gold Nanoparticles as Contrast Agents in Ophthalmic Imaging. *Optics* vol. 4 74–99 Preprint at https://doi.org/10.3390/opt4010007 (2023).
78. Siddique, S. & Chow, J. C. L. Gold nanoparticles for drug delivery and cancer therapy. *Applied Sciences (Switzerland)* vol. 10 Preprint at https://doi.org/10.3390/app10113824 (2020).
79. Baskar, R., Lee, K. A., Yeo, R. & Yeoh, K.-W. Cancer and Radiation Therapy: Current Advances and Future Directions. *Int J Med Sci* **9**, 193–199 (2012).
80. Sutradhar, K. B. & Amin, Md. L. Nanotechnology in Cancer Drug Delivery and Selective Targeting. *ISRN Nanotechnology* **2014**, 1–12 (2014).

81. Yao, C. *et al.* Gold Nanoparticle Mediated Phototherapy for Cancer. *J Nanomater* **2016**, 1–29 (2016).
82. Zharov, V. P., Mercer, K. E., Galitovskaya, E. N. & Smeltzer, M. S. Photothermal Nanotherapeutics and Nanodiagnostics for Selective Killing of Bacteria Targeted with Gold Nanoparticles. *Biophys J* **90**, 619–627 (2006).
83. Colombeau, L. *et al.* Inorganic Nanoparticles for Photodynamic Therapy. in 113–134 (2016). doi:10.1007/978-3-319-22942-3_4.
84. Hainfeld, J. F., Dilmanian, F. A., Slatkin, D. N. & Smilowitz, H. M. Radiotherapy enhancement with gold nanoparticles. *Journal of Pharmacy and Pharmacology* **60**, 977–985 (2010).
85. Daraee, H. *et al.* Application of gold nanoparticles in biomedical and drug delivery. *Artif Cells Nanomed Biotechnol* **44**, 410–422 (2016).
86. Park, J. H. & Oh, N. Endocytosis and exocytosis of nanoparticles in mammalian cells. *Int J Nanomedicine* 51 (2014) doi:10.2147/IJN.S26592.
87. Chithrani, B. D. & Chan, W. C. W. Elucidating the Mechanism of Cellular Uptake and Removal of Protein-Coated Gold Nanoparticles of Different Sizes and Shapes. *Nano Lett* **7**, 1542–1550 (2007).
88. Zhao, F. *et al.* Cellular Uptake, Intracellular Trafficking, and Cytotoxicity of Nanomaterials. *Small* **7**, 1322–1337 (2011).
89. Chithrani, D. B. Intracellular uptake, transport, and processing of gold nanostructures. *Mol Membr Biol* **27**, 299–311 (2010).
90. Verma, A. & Stellacci, F. Effect of Surface Properties on Nanoparticle–Cell Interactions. *Small* **6**, 12–21 (2010).
91. Qiu, Y. *et al.* Surface chemistry and aspect ratio mediated cellular uptake of Au nanorods. *Biomaterials* **31**, 7606–7619 (2010).
92. Cho, E. C., Xie, J., Wurm, P. A. & Xia, Y. Understanding the Role of Surface Charges in Cellular Adsorption versus Internalization by Selectively Removing Gold Nanoparticles on the Cell Surface with a I_2 /KI Etchant. *Nano Lett* **9**, 1080–1084 (2009).
93. Canton, I. & Battaglia, G. Endocytosis at the nanoscale. *Chem Soc Rev* **41**, 2718 (2012).
94. Rejman, J., Bragonzi, A. & Conese, M. Role of clathrin- and caveolae-mediated endocytosis in gene transfer mediated by lipo- and polyplexes. *Molecular Therapy* **12**, 468–474 (2005).
95. Balasubramanian, N., Scott, D. W., Castle, J. D., Casanova, J. E. & Schwartz, M. A. Arf6 and microtubules in adhesion-dependent trafficking of lipid rafts. *Nat Cell Biol* **9**, 1381–1391 (2007).
96. Mayor, S. & Pagano, R. E. Pathways of clathrin-independent endocytosis. *Nat Rev Mol Cell Biol* **8**, 603–612 (2007).
97. Iversen, T.-G., Skotland, T. & Sandvig, K. Endocytosis and intracellular transport of nanoparticles: Present knowledge and need for future studies. *Nano Today* **6**, 176–185 (2011).

98. Vercauteren, D. *et al.* The Use of Inhibitors to Study Endocytic Pathways of Gene Carriers: Optimization and Pitfalls. *Molecular Therapy* **18**, 561–569 (2010).
99. Ivanov, A. I. Pharmacological Inhibition of Endocytic Pathways: Is It Specific Enough to Be Useful? in 15–33 (2008). doi:10.1007/978-1-59745-178-9_2.
100. Rothen-Rutishauser, B., Bourquin, J. & Petri-Fink, A. Nanoparticle-cell interactions: Overview of uptake, intracellular fate and induction of cell responses. in *NanoScience and Technology* 153–170 (Springer Verlag, 2019). doi:10.1007/978-3-030-12461-8_6.
101. Sousa, A. A. *et al.* Synthesis, Characterization, and Direct Intracellular Imaging of Ultrasmall and Uniform Glutathione-Coated Gold Nanoparticles. *Small* **8**, 2277–2286 (2012).
102. Malatesta, M. Transmission Electron Microscopy as a Powerful Tool to Investigate the Interaction of Nanoparticles with Subcellular Structures. *Int J Mol Sci* **22**, 12789 (2021).
103. Yue, J., Feliciano, T. J., Li, W., Lee, A. & Odom, T. W. Gold Nanoparticle Size and Shape Effects on Cellular Uptake and Intracellular Distribution of siRNA Nanoconstructs. *Bioconjug Chem* **28**, 1791–1800 (2017).
104. Costanzo, M. *et al.* Fluorescence and electron microscopy to visualize the intracellular fate of nanoparticles for drug delivery. *European Journal of Histochemistry* **60**, 107–115 (2016).
105. Shao, X., Meng, C., Song, W., Zhang, T. & Chen, Q. Subcellular visualization: Organelle-specific targeted drug delivery and discovery. *Advanced Drug Delivery Reviews* vol. 199 Preprint at https://doi.org/10.1016/j.addr.2023.114977 (2023).
106. Krichevsky, O. & Bonnet, G. *Fluorescence Correlation Spectroscopy: The Technique and Its Applications*. *ON PROGRESS IN PHYSICS Rep. Prog. Phys* vol. 65 (2002).
107. Ettinger, A. & Wittmann, T. Fluorescence live cell imaging. in *Methods in Cell Biology* vol. 123 77–94 (Academic Press Inc., 2014).
108. Chazotte, B. Labeling Lysosomes in Live Cells with LysoTracker. *Cold Spring Harb Protoc* **2011**, pdb.prot5571 (2011).
109. pHrodo Indicators for pH Determination. *Thermo Fisher Scientific* https://www.thermofisher.com/pt/en/home/brands/molecular-probes/key-molecular-probes-products/phrodo-indicators.html (2017).
110. Meyvis, T. K. L., De Smedt, S. C., Van Oostveldt, P. & Demeester, J. Fluorescence Recovery After Photobleaching: A Versatile Tool for Mobility and Interaction Measurements in Pharmaceutical Research. *Pharm Res* **16**, 1153–1162 (1999).
111. Saxton, M. J. & Jacobson, K. *SINGLE-PARTICLE TRACKING: Applications to Membrane Dynamics*. *Annu. Rev. Biophys. Biomol. Struct* vol. 26 www.annualreviews.org (1997).
112. Shiba, A., Kinoshita-Kikuta, E., Kinoshita, E. & Koike, T. TAMRA/TAMRA Fluorescence Quenching Systems for the Activity Assay of Alkaline Phosphatase. *Sensors* **17**, 1877 (2017).

113. Hollmann, B., Perkins, M., Chauhan, V. M., Aylott, J. W. & Hardie, K. R. Fluorescent nanosensors reveal dynamic pH gradients during biofilm formation. *NPJ Biofilms Microbiomes* **7**, 50 (2021).
114. Le Guern, F., Mussard, V., Gaucher, A., Rottman, M. & Prim, D. Fluorescein Derivatives as Fluorescent Probes for pH Monitoring along Recent Biological Applications. *Int J Mol Sci* **21**, (2020).
115. Sahoo, S. K., De, T. K., Ghosh, P. K. & Maitra, A. pH- and Thermo-sensitive Hydrogel Nanoparticles. *J Colloid Interface Sci* **206**, 361–368 (1998).
116. Chaudhari, R. D., Joshi, A. B., Pandya, K. & Srivastava, R. pH Based Urea Biosensing Using Fluorescein Isothiocyanate (FITC)-Dextran Encapsulated Micro-Carriers of Calcium Alginate. *Sens Lett* **14**, 451–459 (2016).
117. Lee, P. C. & Meisel, D. Adsorption and surface-enhanced Raman of dyes on silver and gold sols. *J Phys Chem* **86**, 3391–3395 (1982).
118. Drobnica, ., Kristin, P. & Augustn, J. The chemistry of the- NCS group. in *Cyanates and Their Thio Derivatives: Vol. 2 (1977)* 1003–1221 (John Wiley & Sons, Ltd., Chichester, UK). doi:10.1002/9780470771532.ch6.
119. Brown, K. K. & Hampton, M. B. Biological targets of isothiocyanates. *Biochimica et Biophysica Acta (BBA) - General Subjects* **1810**, 888–894 (2011).
120. Kala, C., Salman Ali, S., Ahmad, N., Jamal Gilani, S. & Ali Khan, N. Isothiocyanates: a Review. *Research Journal of Pharmacognosy (RJP)* **5**, 71–89 (2018).
121. Chen, W., Zhao, Y., Seefeldt, T. & Guan, X. Determination of thiols and disulfides via HPLC quantification of 5-thio-2-nitrobenzoic acid. *J Pharm Biomed Anal* **48**, 1375–1380 (2008).
122. Aitken, A. & Learmonth, M. Estimation of Disulfide Bonds Using Ellman's Reagent. in 487–488 (1996). doi:10.1007/978-1-60327-259-9_82.
123. Selvan, S. T., Tan, T. T. Y., Yi, D. K. & Jana, N. R. Functional and Multifunctional Nanoparticles for Bioimaging and Biosensing. *Langmuir* **26**, 11631–11641 (2010).
124. Yavuz, M. S. *et al.* Gold nanocages covered by smart polymers for controlled release with near-infrared light. *Nat Mater* **8**, 935–939 (2009).
125. Xie, J., Lee, S. & Chen, X. Nanoparticle-based theranostic agents. *Adv Drug Deliv Rev* **62**, 1064–1079 (2010).
126. Hu, M. *et al.* Gold nanostructures: engineering their plasmonic properties for biomedical applications. *Chem Soc Rev* **35**, 1084 (2006).
127. Shi, X. *et al.* Spectroscopic investigation of the interactions between gold nanoparticles and bovine serum albumin. *Chinese Science Bulletin* **57**, 1109–1115 (2012).
128. Storhoff, J. J., Elghanian, R., Mucic, R. C., Mirkin, C. A. & Letsinger, R. L. One-Pot Colorimetric Differentiation of Polynucleotides with Single Base Imperfections Using Gold Nanoparticle Probes. *J Am Chem Soc* **120**, 1959–1964 (1998).

129. Yu, H. & Jiang, D. [Spectroscopic studies on electrostatically self-assembled gold nanoparticulate thin films]. *Guang Pu Xue Yu Guang Pu Fen Xi* **22**, 511–4 (2002).
130. Baptista, P., Doria, G., Henriques, D., Pereira, E. & Franco, R. Colorimetric detection of eukaryotic gene expression with DNA-derivatized gold nanoparticles. *J Biotechnol* **119**, 111–117 (2005).
131. Sperling, R. A. & Parak, W. J. Surface modification, functionalization and bioconjugation of colloidal inorganic nanoparticles. *Philosophical Transactions of the Royal Society A: Mathematical, Physical and Engineering Sciences* **368**, 1333–1383 (2010).
132. Stewart, R. & Yates, K. The Position of Protonation of the Carboxyl Group [1]. *J Am Chem Soc* **82**, 4059–4061 (1960).
133. Xu, L., Li, B. & Jin, Y. Inner filter effect of gold nanoparticles on the fluorescence of quantum dots and its application to biological aminothiols detection. *Talanta* **84**, 558–564 (2011).

APPENDIXES

A.1 Ellman's Assay

In order to determine the number of PEG molecules that did not bind to the AuNPs, the Ellman's assay was performed. This assay relies on the reaction between free thiol groups with the Ellman's reagent (DTNB), releasing TNB. Then, absorbance readings at 412 nm allows the quantification of TNB molecules. In order to perform the Ellman's assay, a calibration curve was drawn. For that, samples with known concentration of PEG were prepared, in the presence of DTNB, and analysed by UV-Visible spectroscopy. The quantification of unbound PEG molecules was obtained by analysing the resulting supernatants during the functionalization.

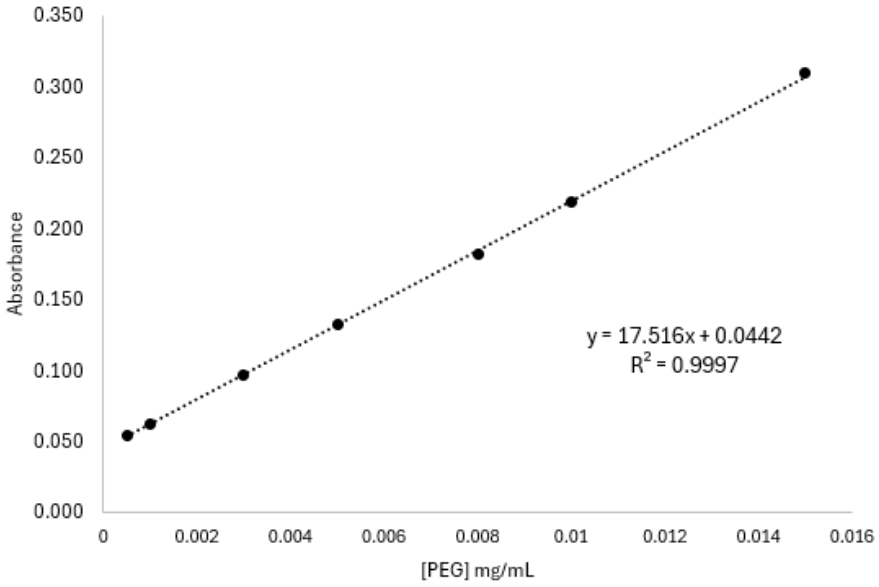

Figure A.4.1 Standard calibration curve of PEG chains used in the Ellman's Assay, obtained by UV-Vis spectroscopy

A.2 Quantification of Excess TAMRA Molecules by Fluorescent Spectroscopy

To determine the excess of TAMRA that did not bind to the AuNPs, a calibration curve was drawn, with the preparation of samples ranging from 0 – 0.01 mg/mL in 2.5 mM MES buffer pH 5.9, in the conditions of functionalization. Fluorescent spectroscopy was used to quantify the fluorescent intensity, which was plotted in function of TAMRA concentrations (Figure A.2). After functionalization, supernatants were recovered and analyzed under the same conditions, and the amount of TAMRA was calculated by interpolating the calibration curve. All readings were taken in the established work conditions.

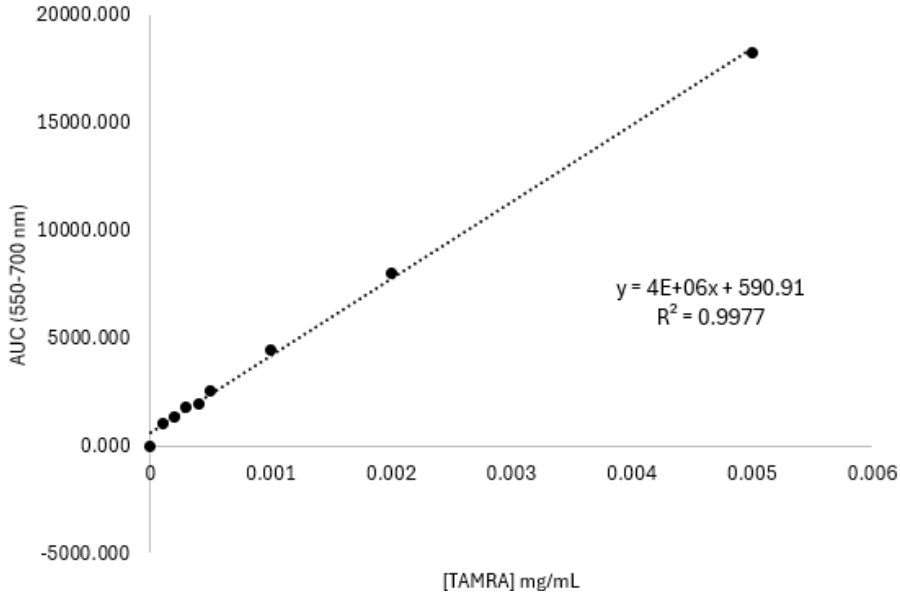

Figure A.4.2 Standard TAMRA concentration calibration curve obtained by Fluorescent Spectroscopy

A.3 Quantification of Excess FITC Molecules by Fluorescent Spectrosocpy

To determine the excess of FITC that did not bind to the AuNPs, a calibration curve was drawn, with the preparation of samples ranging from 0 – 0.003 mg/mL in 0.1 M carbonate buffer pH 9.34, in the conditions of functionalization. Fluorescent spectroscopy was used to quantify the fluorescent intensity, which was plotted in function of FITC concentrations (Figure A.3). After functionalization, supernatants were recovered and analyzed under the same conditions, and the amount of FITC was calculated by interpolating the calibration curve. All readings were taken in the established work conditions.

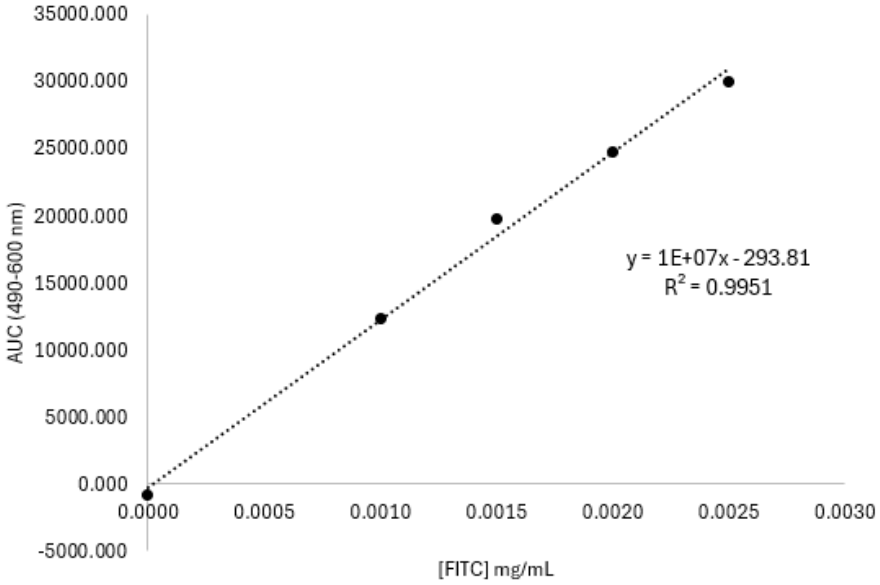

Figure A.4.3 Standard FITC concentration calibration curve obtained by Fluorescent Spectroscopy

A.4 Macrsocopic Analysis of AuNP samples after incubation in different pH values

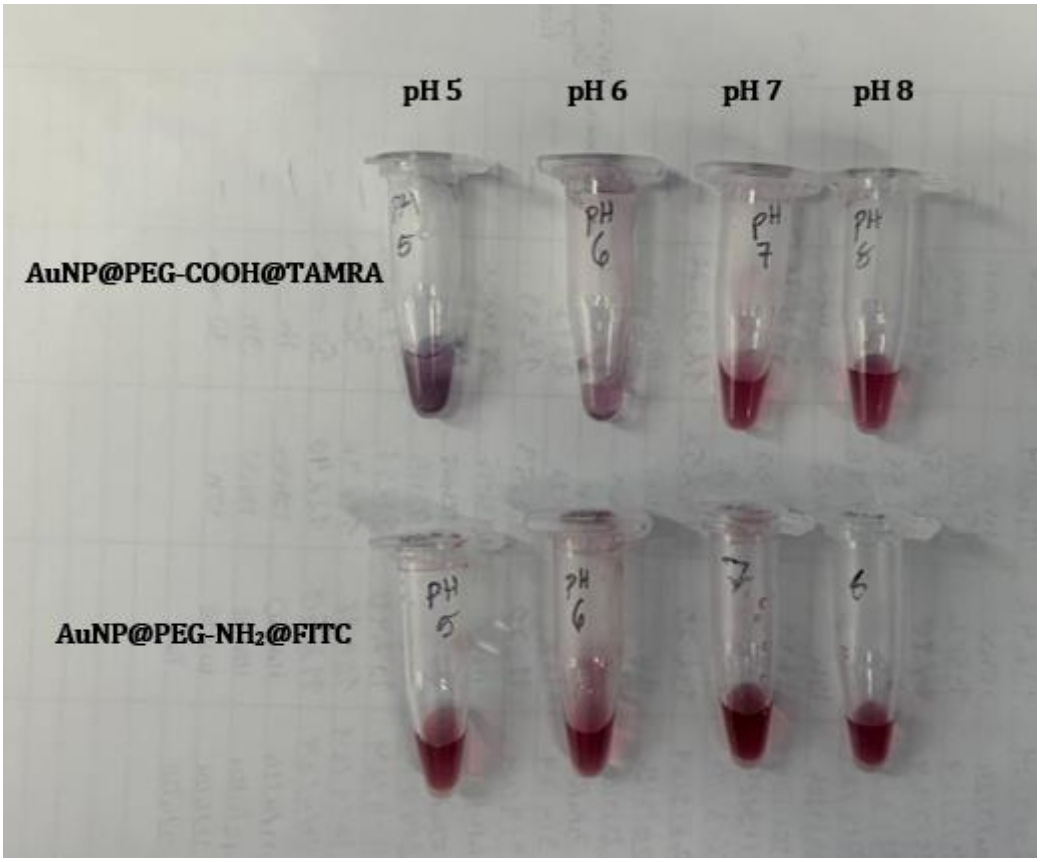

Figure A.4.4 Functionalized AuNP samples used in the pH Stability assay. AuNP@PEG-COOH@TAMRA samples at pH 5 and 6 completely lost their characteristic red colour, turning blue/purple.